CHARACTERIZATION AND COMPARISON OF WHITE LAYER BY HARD TURNING VERSUS GRINDING

by

JASDEEP SINGH SAHNI

A THESIS

Submitted in partial fulfillment of requirements
for the degree of Master of Science
in the Department of Mechanical Engineering
in the Graduate School of
The University of Alabama

TUSCALOOSA, ALABAMA

2004

To...

My parents, Ranjit S. Sahni and Amarjit K. Sahni,

and my sister's Ramandeep K. Sahni and Aman Sahni

Submitted by Jasdeep Singh Sahni in partial fulfillment of the requirement for the degree of Master of Science specializing in Mechanical Engineering.

Accepted on behalf of the Faculty of the Graduate School by the thesis committee:

Mark L. Weaver, Ph.D.

Kevin Chou, Ph.D.

Yuebin Guo, Ph.D.
Chairperson

William H. Sutton, Ph.D.
Department Chairperson

1/25/03
Date

Ronald W. Rogers, Ph.D.
Dean of the Graduate School

12/22/03
Date

LIST OF ABBREVIATIONS AND SYMBOLS

WL	White Layer
DL	Dark Layer
TEM	Transmission Electron Microscopy
SEM	Scanning Electron Microscopy
XRD	X-ray Diffraction
XPS	X-ray Photospectroscopy
UTM	Untempered Martensite
OTM	Overtempered Martensite
FCC	Face Centered Cubic
BCC	Body Centered Cubic
Ms	Martensite Start Temperature
M_f	Martensite Finish Temperature
TTT	Time Temperature Transformatio
α	Ferrite (martensite) phase
$\acute{\alpha}$	tempered martensite phase
γ_R	Retained austenite phase
γ	Austenite Phase
Fe_3C	Iron Carbide (cememtite)
Fe_3O_4	Iron Oxide
^oC	Degree Centigrade

F	Fahrenheit
BHN	Brinell Hardness Number
HRC	Rockwell Hardness Number
CBN	Cubic Boron Nitrite
NC	Numerical Control
CNC	Computer Numerical Control
AISI	American Iron and Steel Institute
nm	Nanometer
Ac_3	Upper Critical Temperature
Al_2O_3	Aluminium Oxide
KV	Kilovolt
µm	Micrometer
eV	Electron volt
keV	Kilo electron volt

ACKNOWLEDGMENTS

I would like to express my sincere gratitude to my advisor Dr. Yuebin Guo, for his technical guidance, support and for being constant source of encouragement throughout the course of this research. Sincere thanks are extended to Dr. Mark L. Weaver and Dr. Kevin Chou for agreeing to serve in my thesis committee and for providing valuable suggestions during the course of this research work and writing thesis. Special thanks are due to Dr. Mohammed Shamsuzzoha for his help provided for TEM experimental and analysis work.

I am thankful to Dr. James Weston for giving fruitful suggestions regarding X-ray diffraction analysis. I would like to thank Dr. Gregg M. Janowski at Department of Metallurgical Engineering at University of Alabama at Birmingham for X-ray diffraction studies. The assistance of Ms J. Liu and Mr. G.Q. Wang on SEM and Dr. J.Y. Zhang on XPS analysis is greatly appreciated.

Facilities are imperative for conducting research work. I am pleased to extend my thanks to Mr. David Gann at NACCO Material Handling Group for providing cutting inserts. I am thankful to Sam Tingle, Kenneth Dunn, Bobby Edmonds, Joe Howell, and Barry Johnson at the Machine Shop for facilities provided for machining. I am thankful to Dr. Mikhael Bersh of School of Mines and Energy Development at The University of Alabama for providing Optical Microscope. Mr. Larry Smith and Mr. Robert Fanning of Department of Metallurgical and Materials engineering are highly appreciated for their

time and help provided for use of research facilities during the course of this research work. Finally I would like to convey my thanks to the faculty, staff and students of Department of Mechanical Engineering at The University of Alabama for providing me academic and working environment to successfully finish my research work.

Last but not the least, I am thankful to my friends Sumandeep Singh Shergill, Vikas Grover, Sushil Sehgal, Parshant Dhand, and Amit Madan for making my stay pleasant in Tuscaloosa.

CONTENTS

LIST OF TABLES

LIST OF FIGURES

ABSTRACT

Compared with grinding, hard turning has the potential to make a variety of precision components of superior surface integrity, such as bearings, gears, cams, shafts, tools, dies, etc., while reducing investment, increasing production rate, and eliminating environmental pollution. Despite its spectrum of advantages over cost intensive grinding process, industrial realization of hard turning still remains in incipient stage. The low industrial acceptance of hard turning may be attributed to uncertainty related to surface quality especially for the white layer which is a key factor of surface integrity and thus product performance.

A comparative study has been conducted to solve the current problems. Hard turning and grinding AISI 52100 (62 to 64 HRC) steel were designed and conducted to generate the white layer. Then, white layer induced by hard tuning and grinding were characterized and compared in six aspects: (1) Surface structure by optical microscope; (2) Hardness by microhardness tester; (3) Microstructure by scanning electron microscopy (SEM); (4) Chemical composition by X-ray photo spectroscopy (XPS); (5) Retained austenite phase by X-ray diffraction; (6) Crystal defects and microstructure by Transmission Electron Microscopy (TEM).

The experimental results have shown that: (a) characteristics of the surface structures by hard turning and grinding are fundamentally different. Further, abusive grinding tends to induce much thicker white layer than abusive hard turning; (b) the

ground white layer is about 10% harder than that of turned one, but the ground dark layer seems to be softer than the turned one. Further, etching seems to affect the hardness of dark layer and corresponding effect in white layer is not noticeable. (c) the ground white layer is etched and therefore shows clear microstructures in a SEM image, while the turned one is etch resistant and shows featureless structures. The ferrite matrix of the ground dark layer is much more severely etched than the turned one. Additionally, the turned white layer appears much more strained in cutting direction than the ground one; and (d) both the turned and ground white layers are rich in oxygen or at least oxide-rich. The turned white layer has increased carbon and reduced oxygen concentrations, while the ground one behaves just opposite. (e) the percentage of retained austenite in ground white layer is much less than in turned white layer. No retained austenite was detected in ground dark layer as compared to 14 % in turned dark layer. (f) TEM study revealed that a large number of precipitates in turned and ground white layer as compared to bulk and untempered material. This suggests that precipitation has occurred due to rapid heating and quenching. The large number of defect bands in ground white layer as compared to turned white layer suggests that former has fine grain size as compared to later.

CHAPTER 1

INTRODUCTION

Hard turning is an emerging technology to machine the steel in hardened state. It is known to have potential to replace grinding as a finishing operation. It is defined as turning of hardened steel with hardness greater than 30 HRc. It originated out of the automotive industry's need to machine hardened steel at a much faster rate to increase productivity. It was in early 50's USA, 70's in Germany, and 80's in Japan the hard turning first began to replace grinding processes for components made of hardened steel. Significant advantages of hard turning are shorter machining time, shorter production sequence, lower production cost, and smaller batch size. It can eliminate grinding when machining hardened steel parts like roller bearing rings, precision gears, and injection valves, saving both time and money. Since hard turning requires no coolant, the process not only saves money but also eases environmental concerns: no coolant to dispose of and no grinding slurry to worry about. Despite its spectrum of advantages over cost intensive grinding process, industrial realization of hard turning still remains in incipient stage. The low industrial acceptance of hard turning may be attributed to uncertainty related to surface quality. For it to be accepted as substitute to grinding, the properties of the surface and subsurface layers and their effect on performance on fatigue life of

components have to be well understood and established. Although hard turning is generally considered more expensive than conventional finishing methods, recent advances in tooling and techniques are gradually changing these perceptions. As questions about its ability to meet surface finish and integrity requirements are answered, finish hard turning will be more widely recognized as a cost-effective alternative to grinding in many cases. Greater flexibility, faster tool changes and longer tool life contribute to lower machining costs, higher productivity and better part quality and far outweighing the initial cost of (PCBN) tools.

Machined parts are used in various applications. So reliability of the machined part needs utmost importance since a failure of small part can cause tremendous loss of life of property in applications such as airplanes. It is well known that most of machined parts fail due to crack formation. Surface of machined part has a great bearing on part performance.

It is well known that a white layer can be formed on the hard turned and ground surface. White layer is found to be present in variety of situations and service environments like leaf springs, roller bearings, piston rings, punching, blanking, reaming, drilling, milling, etc [Griffiths, 85]. In fact there are as great a variety of white layer structures, forms and types as there are formation situations [Griffiths, 86]. Grozin [62] found seven different types of white layer and emphasized that structure of white layer found in various situation may be different depending upon how it was formed, materials and environment. Turley [75] found the structure of white layer by reaming and grinding to be different, however there is no consensus regarding many crucial properties of white layer. There are many conflicting opinions relating to microstructure, hardness,

composition and formation mechanism, of white layer and their effect on product performance and fatigue life. Some work showed that the presence of white layer increases the fatigue life of components [Tönshoff, 95, Field, 70], on the other hand some reported that despite white layer occurrence, hard turned steels have greater fatigue life [Abrão, 96]. Two conflicting opinions exist regarding wear resistance of surface with white layer. Griffiths [87] postulated higher wear resistance of surface having white layer. In contrast Yang [20] found reduced wear resistance due to presence of white layer. In either case, white layer properties play an important role in component performance. Shaw [16] termed the presence of white layer on the surface as an important unacceptable surface defect. Abrão [96] addressed the surface integrity of turned and ground surface but no white layer was obtained in ground sample probably because grinding conditions employed were extremely gentle. Since it is known that the underlying mechanism of hard turning and grinding are different, it would be expected that white layer formed by two competing processes is different. No through comparison of properties of white layer produced in hard turning and grinding. This lacking of white layer comparison would significantly block potential industrial applications of hard turning. Thus a white layer comparison for hard turning versus grinding would provide useful data for manufactures to select an appropriate process for their particular operations and needs. The present study of white layer was undertaken to compare and characterize white layer by hard turning vs grinding. Hard turning and grinding AISI 52100 (62 to 63 HRc) steel experiments have been designed and conducted to generate thick white layers for reliable measurement. Then white layer characteristics were compared with respect to their hardness by microhardness tester, surface structure by optical microscope, microstructure

by SEM, chemical composition by XPS, volume fraction of retained austenite by XRD, crystal structure and defects by TEM.

CHAPTER 2

BACKGROUND

This chapter introduces the hard turning and grinding process and their relative merits and demerits. This is followed by introduction to concept of surface integrity. Finally physically metallurgy and heat treatment of steel is discussed with particular attention on the austenite-martensite phase transformation. The chapter concludes with a discussion of the metallurgical changes occurring at the surface of hardened steel by machining and grinding.

2.1 Turning

Turning is the machining operation in which a single point tool removes material from the surface of a rotating cylindrical workpiece. Turning is traditionally carried out on a lathe, which provides power to turn the part at a given rotational speed and to feed the tool at a specified rate and depth of cut. Figure 2.1 shows the schematics of turning operation. The workpiece is held in a rotating chuck which is mounted on a spindle.

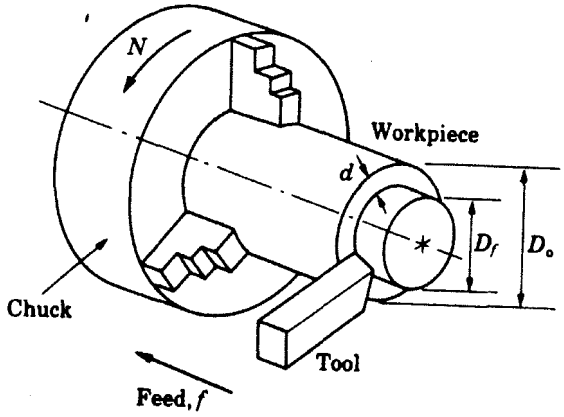

Figure 2.1 Turning Operation [Kalpakjian, 92]

2.2 Grinding

Grinding is a machining operation in which a multi edged rotating abrasive tool called grinding wheel removes material from a translating workpiece (surface grinding) or a rotating workpiece (cylindrical grinding) as shown in Figure 2.2.

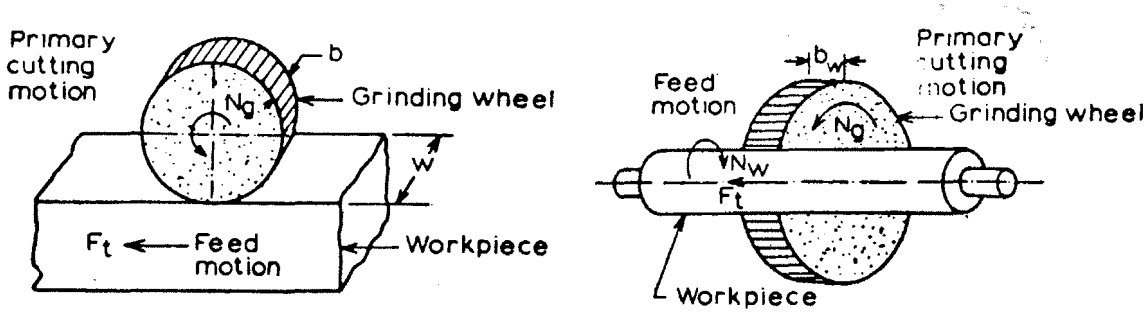

(a) Surface Grinding (b) Cylindrical Grinding

Figure 2.2 Grinding Operation [Juneja, 95]

2.3 Hard Turning Vs Conventional Turning

By definition, the main difference between hard turning and traditional turning is in the hardness of the workpiece. However, the difference in hardness of workpiece necessitates the use of different process parameters for hard turning. So many other differences can be enlisted between hard turning and conventional turning. The cutting mechanism of hard turning is different from that of machining soft steel. As a finishing or semi-finishing operation, the depth of cut and the feed are fairly small. Cutting tools with relatively large cutting edge radius or chamfer are normally used. Thus, the chip formation takes place exclusively in the corner radius and on the chamfer of the cutting tool [König, 93]. In addition, a chamfered cutting edge is used to reduce the chipping of the cutting edge. The machined surface of soft steel does not seem to undergo any phase transformation while on the other hand the existence of white and dark layer on hard turned surface is well known. Figure 2.3 shows the typical geometrical conditions in hard turning. The special features of hard turning process are negative rake angle, saw toothed chips, high ratio of thrust to cutting force component, relatively low specific energy consumption, and low cutting forces.

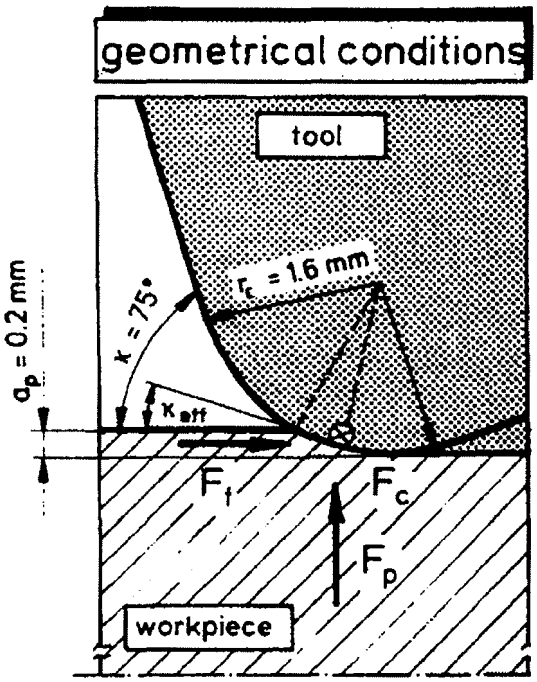

Figure 2.3 Geometrical Conditions in Hard Turning [Tönshoff et al., 95]

2.4 Hard Turning Vs Grinding

Compared with grinding, hard turning is competitive in making a variety of precision components with substantial potential benefits. However, resistance to use hard turning is very real since surface integrity has not been well understood, especially the properties of the white layer induced in hard turning and grinding. Further, the white layer is often presumed detrimental to fatigue life. As grinding manufacturers are keeping pace with industry, it may be difficult to prove conclusively that hard turning is preferential to grinding. The common feature of hard turning and grinding is the negative rake angle of the tool in hard turning and abrasive grain in grinding. There are many aspects of distinction between hard turning and grinding [König, 93]: (1) The contact length between grinding wheel and the workpiece is usually several times larger than that

between the tool wear land and the workpiece in hard turning. Further, surface grinding speed is much larger than that in hard turning. Therefore, there is great chance for thermal damage in grinding; (2) Contact time and time for heat conduction are much longer in grinding than in turning, which makes high temperatures penetrate deep into the workpiece, resulting in a thick ground white layer; (3) The average stress over the entire contact length in grinding is less than in hard turning. High levels of compressive stress occur only in the area around individual grain contact. These contact areas are small in comparison with the tool wear land which occurs in hard turning; and (4) The penetration depth of residual compressive stress caused by Hertzian stress in the grinding operation is less than that in hard turning. These factors indicate that the physical properties of a ground white layer may differ significantly in many aspects from those of a turned one. Therefore, differences are also expected in product performance such as rolling contact fatigue life.

2.4.1 Advantages of Hard Turning

Hard turning has lot of advantages from industrial point of view. It is known to have potential to replace grinding as finishing operation due to following reasons:

- Hard turning is usually preferred over grinding when shape of workpiece is very complex or when we are combining several operations using a NC machine. For example, hard turning is used to cut splines in output/input shafts of material of hardness about 62HRC, which require deep grooves. The CBN tool makes a straighter groove than grinding.

- Machine tools are less expensive for hard turning. A CNC cylindrical grinder costs at least twice as much as a CNC lathe.
- Hard turning continues to be increasingly competitive with grinding and dimensional tolerances and surface finishes are beginning to approach those obtained with grinding.
- The energies consumed in grinding are 10 to 100 times those consumed in turning.
- In turning we don't need to balance the tool, but in grinding we have to balance the grinding wheel.
- Grinding process is more complex than turning as turning hass parameters involved.
- Thermal and other damage to the workpiece surface is more likely to occur in grinding. Hard part turning may avoid grinding burns and microscopic edge cracks, and produces compressive residual stresses on the surface which leads to improved life of the part.
- In hard turning there is no need for coolant because 90% of the heat goes off in the chip where as in grinding coolant is needed. Use of coolant is considered hazardous to environment. Also with use of coolant there is a need for mist collectors to prevent fire hazard.
- Also the use of high speed grinders requires high safety measures and grinders have to be approved which is not the case with turning tools.

2.4.2 Limitations of Hard Turning

- Operators for hard turning need to have mindset for precision operation.
- The grinding process has truing and dressing, which makes the process stable and easy to control. But single point cutting tools unfortunately wear gradually, and in some way

they are not stable. So turning tool has to be checked regularly based on experience and changed when the wear is excessive.

- Workholding devices for large and slender workpieces during hard turning can present significant problems because the cutting forces used are higher than grinding forces.

Competitive position of hard turning Vs grinding must be evaluated individually for each application and in terms of product surface finish and integrity, quality and overall economics.

2.5 Physical Metallurgy of Steel

Steel is an alloy of iron and iron carbide. Depending upon the carbon content, alloying elements and thermal processing, steel can exhibit variety of microstructures and properties. This makes it useful in variety of applications. The iron-carbon equilibrium diagram Figure 2.4 shows the phase composition and structure of alloys in the carbon content range from pure iron to cementite (6.67 % C). A phase is related to any homogeneous mechanically separable constituents of an alloy; and in steel there are three important phases; ferrite, cementite and austenite. Alloys of iron containing up to 2.14 % C are known as steels and those containing over 2.14 % C are known as cast irons. The essential difference between cast iron and steel is that steel never contains graphite or free carbon. Carbon exists in very small quantity in ferrite and majority in cementite.

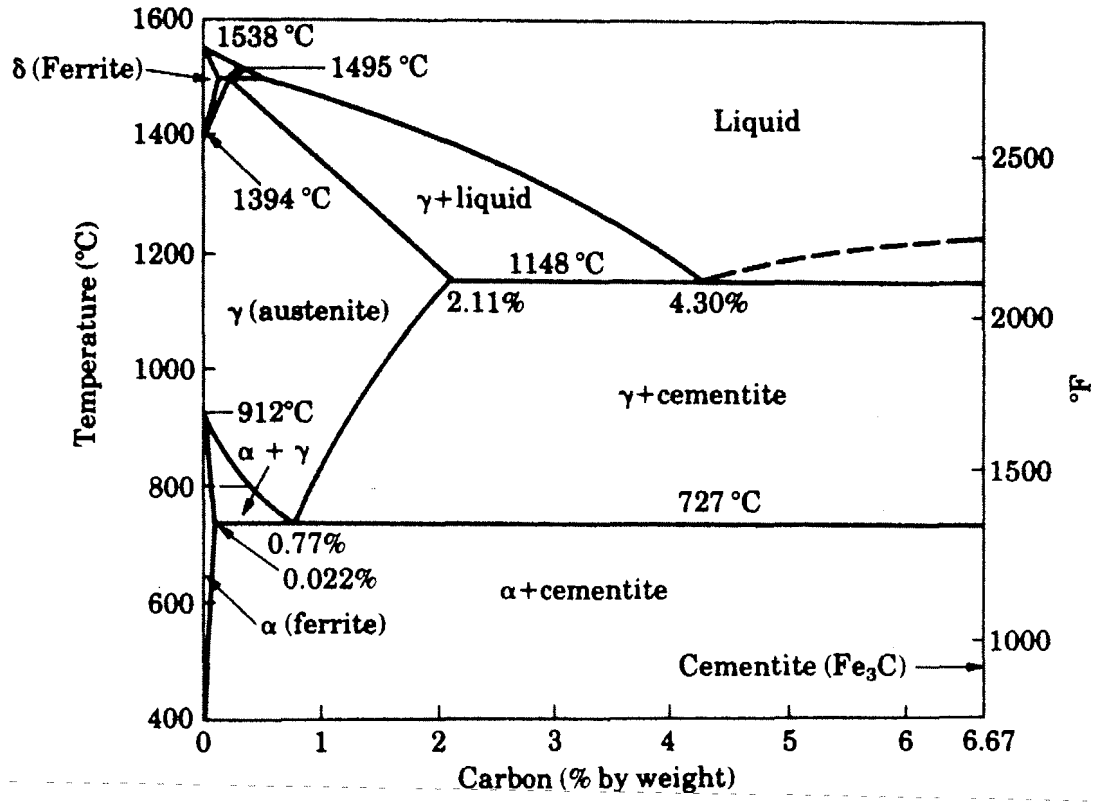

Figure 2.4 Iron-Carbon Phase Diagram [Kalpakjian, 92]

There are six main phases of steel: ferrite, cementite, austenite, martensite, pearlite and bainite:

Ferrite is the solid solution of carbon and other constituents in α-iron. It is soft week and is most prominent for its high ductility. The hardness of ferrite is in range of 50-100 BHN. In Iron carbon phase diagram, distinction is made between low temperature α-ferrite with carbon solubility up to 0.02 % and high temperature δ-ferrite with a maximum carbon solubility of 0.1%. Carbon atoms are also located in the vacancies on the dislocations, etc. Under a microscope, ferrite is seen as homogeneous polyhedral grains.

Austenite is the solid solution of carbon and other constituents in γ-iron. It has a face centre cubic (FCC) atomic structure which can contain up to 2.14% carbon in solution. Austenite has high ductility, low yield and tensile strength and is non magnetic. The microstructure is made up of polyhedral grains. Austenite is stable only above 1333F (1090°C) in a plain carbon steel, but the presence of certain alloying elements, such as nickel and manganese, stabilizes the austenitic form, even at normal temperatures.

Cementite is the chemical compound of iron and carbon: iron carbide Fe_3C with carbon content being 6.67 %. Cementite has complex rhombic lattice with close packed atoms. Typical features of cementite are its high hardness and low ductility.

Martensite is supersaturated interstitial solid solution of carbon in α-iron and is formed by diffusionless process when steel is cooled rapidly from austenite. The cooling rate should be greater than critical cooling rate for its formation. The FCC structure of austenite rapidly changes to BCC structure of martensite leaving insufficient time for the carbon to form pearlite. Under the microscope in cross section it appears, and is often described, as acicular or needle like, but in 3 dimensions is actually either lathe or plate in structure. Alloys with less than 0.6 percent carbon form lathe martensite. Alloys with more than 1 percent carbon form plate martensite and alloys with from 0.6 to 1.0 percent carbon form mixtures of the two in varying degrees. The hardness of martensite is solely dependant on carbon content and it is normally very high, unless the carbon content is exceptionally low.

Pearlite is a product of eutectoid transformation of austenite. Pearlite is made up of lamellae of ferrite and cementite. Pearlite is relatively soft, ductile and is easily machinable.

Bainite, similar to pearlite, is a mixture of the ferrite and cementite phases. But unlike pearlite, the ferrite and cementite are present in non lamellar arrays whose characteristics are dependent upon alloy composition and transformation temperature. Similar to martensite, the ferrite and bainite may be in the form of laths or plates containing a dislocation structure [Kruss, 80]. Depending on the temperature of formation of bainite it is classified as upper or lower bainite. Upper bainite is formed in temperature range of 250-550°C. Lower bainite is formed at temperature near to martensite start temperature (M_s).

2.5.1 Effect of Alloying Elements

The major alloying elements of 52100 bearing steel used in this study are carbon (1.02%), chromium (1.52%) and manganese (0.34%). Carbon is the most important alloying element in steel. It has profound effect not only on the properties of steel but also on the way in which these can be altered by heat treatment. Iron and carbon combine together to form a compound called iron carbide (Fe_3C) in which one carbon atom is bonded to three iron atoms. In the structure of iron carbon alloys, the carbide is usually called cementite. The amount of cementite present in an iron-carbon alloy depends on the carbon content. If carbon is not present (or present in small traces), the microstructure consists of uniform grains of ferrite (pure BCC iron, with a very small carbon in solution) which is soft and ductile due to absence of cementite. Carbon stabilizes austenite and thereby increases the range of austenite formation in steel. The solubility of carbon in ferrite is limited and it reaches 2.11% at 1148°C. Most of alloying elements present in steel lower the martensite start temperature (Ms). Some of the elements present in steel

are austenite stabilizers (e.g. manganese and nickel), and some are ferrite stabilizers (e.g. silicon, chromium and niobium), and some are strong carbide formers (titanium, niobium, molybdenum and chromium, if present in sufficient quantity) [Kruss, 80]. Chromium is the most important element after carbon. The addition of chromium results in formation of various carbides of chromium which are very hard, yet the steel is more ductile than a steel of the same hardness produced by simple increase in carbon content. Chromium considerably improves corrosion resistance in steels by creating a chromium oxide layer film on the surface. Manganese plays a key role because of two important properties: its ability to combine with sulphur and its powerful deoxidation capacity. It lowers the temperature at which austenite transforms into ferrite, thus avoiding cementite precipitation at ferrite grain boundaries, and by refining the resulting pearlitic structures.

2.5.2 TTT Diagram

The iron-carbon phase diagram in Figure 2.4 indicates the phases of iron and iron carbon (cementite) present under equilibrium conditions. It assumes that the cooling from high temperature has been slow enough to permit austenite to decompose into a mixture of ferrite and cementite at room temperature. This decomposition reaction requires diffusion and other processes that depend on time and temperature. However under conditions of rapid cooling such as in many of the heat treatment processes and in machining and grinding, austenite follows diffusionless process and transforms into nonequilibrium phase called martensite. The nature of martensite transformation can be best understood using the time-temperature-transformation (TTT curve) as shown in Figure 2.5. These diagrams describe the transformation of austenite on cooling at various

cooling rates. The shape of the curve shown varies with composition of steel. The TTT curve shows how cooling rate affects the transformation of austenite into various possible phases. There are two curves in the figure which represent the beginning and end of transformation.

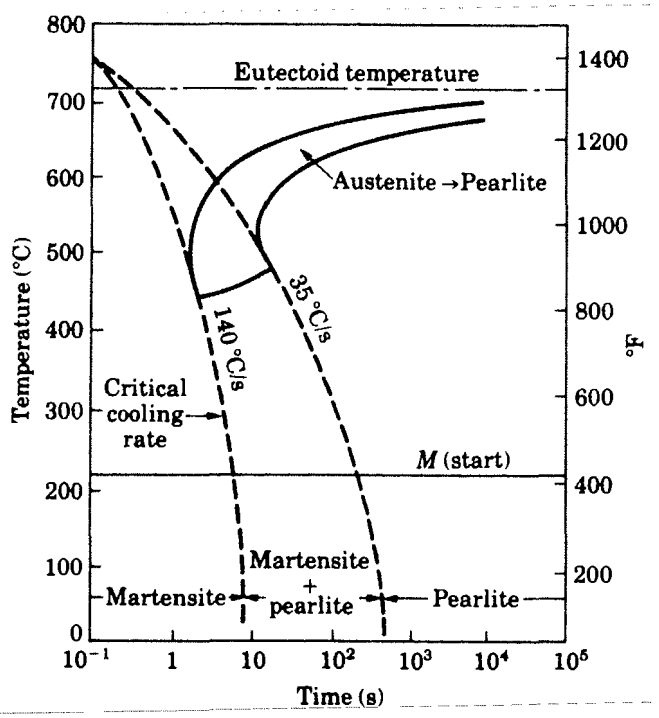

Figure 2.5 TTT Diagram for Steel [Kalpakjian, 92]

At slow cooling rates, the trajectory proceeds through the region indicating transformation into pearlite and bainite, which are alternative forms of ferrite-carbide mixtures. If cooling occurs at a sufficiently rapid rate such as in case of machining and grinding, austenite is transformed into martensite. The face centered cubic structure of austenite is transformed into the body centered tetragonal (BCT) structure of martensite by diffusionless process almost instantly. The temperature at which martensite begins to form in an alloy is given the designation M_s (martensite start) and the temperature at

which martensite is done forming is M_f as shown in TTT diagram Figure 2.5. The TTT diagram for 52100 bearing steel is shown in Figure 2.6.

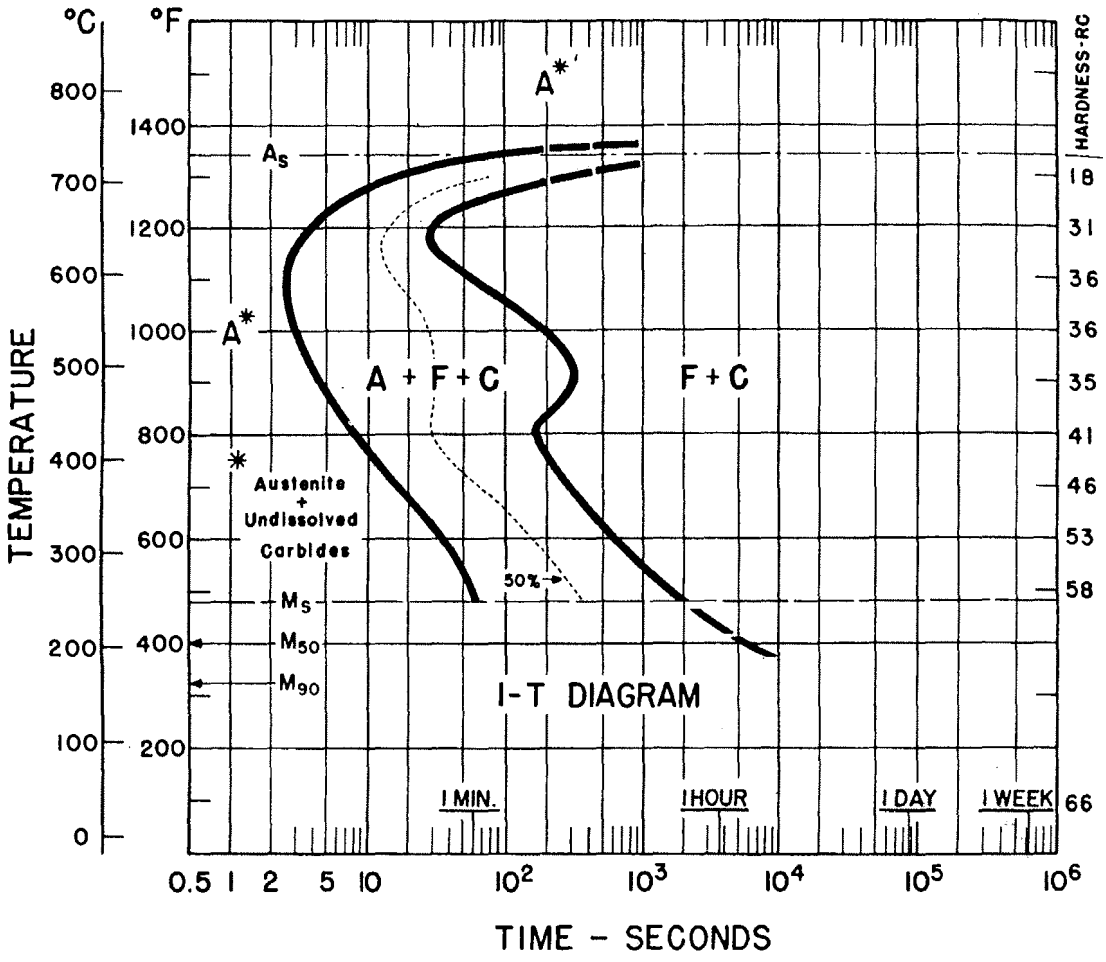

Figure 2.6 Time-Temperature-Transformation diagram for AISI 52100 bearing steel [ASM]

2.6 Heat Treatment of Steel

Heat treatment is the process of heating solid metal to specific degrees of temperature, maintaining heat till saturation and completion of structural changes, and cooling at specific cooling rate to obtain certain physical and mechanical properties, which are associated with changes in the nature, form, size and distribution of the micro-constituents. Steel is heat treated to give it desired mechanical properties. AISI 52100 cold finished, spheriodized and annealed used in this study, had hardness of 183BHN. Steel in this condition is of no industrial uses in application involving contact with between surfaces since soft surface easily wears outs. The material was heat treated (hardened and tempered) to improve its mechanical properties.

Hardening: Hardening is the heat treatment process in which steel is heated to temperature near upper critical temperature, soaking at this temperature for a considerable period to ensure thorough conversion of microstructures, followed by continuous cooling (quenching) to room temperature by quenching in water, oil or brine solution. Final structure of steel produced depends upon the cooling rate employed. If cooling rate is more than critical cooling rate, then a martensite structure is formed. Hardness of steel is due to this structure. The hardness produced by hardening treatment depends on the carbon content of steel. Steel containing less than 0.15% carbon do not respond to hardening treatment.

Tempering: Tempering is a heat treatment operation in which steel hardened by quenching is reheated below sub critical temperatures to modify its properties for the purpose of increasing its usefulness. Such a reheating permits the trapped martensite to

transform to other structures depending upon the tempering temperature. Tempering relieves internal stresses and toughness and ductility are improved at the expense of harness and strength.

2.7 Temperatures in Metal Cutting

In metal cutting process, the energy required for material removal operation is obtained in form of mechanical energy from the motor. The energy supplied by motor is used to deform the material to desired shape. The material is subjected to various strains due to which the material is deformed plastically. When a material is deformed plastically, most of energy is converted into heat in high cutting speeds due to which high temperatures are generated in the interface between tool cutting edge and workpiece surface. The temperature factor is important in machining because of it effects on the tool properties, stresses and microstructural changes on component surface. There are three principal regions of heat generation in machining Figure 2.7. First is the shear zone or primary deformation zone AB, where the heat is generated due to shearing of workpiece material. Second is the interface between the chip and rake face of the tool called secondary deformation zone BC. A third source is the interface between the flank of the tool machined surface of workpiece BD. Most of heat generated at the primary and secondary shear zones is carried away with the chip. The major heat source causing temperature rise of workpiece surface is the interaction between flank of tool and machined surface. This heating effect is due to friction between the surface of workpiece and the flank of the tool.

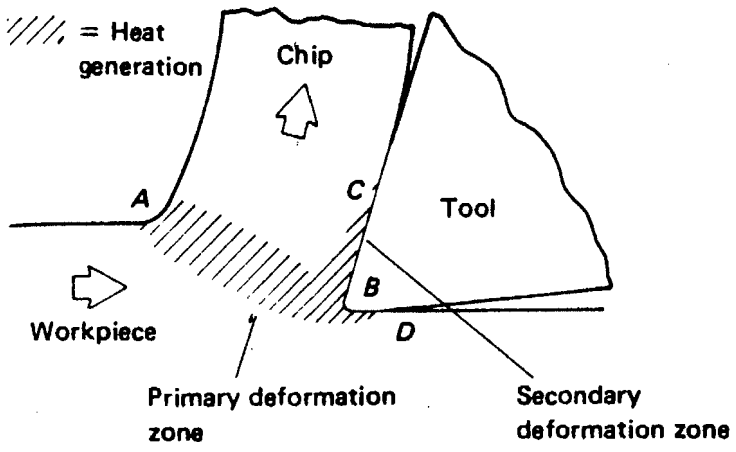

Figure 2.7 Temperature Zones in Metal Cutting [Juneja, 95]

The thermal history of formation of white layer with possibly untempered martensite structure is essentially the same as that which occurs in heat treatment but with two important differences: 1) a very short time for carbon atoms to diffuse uniformly throughout the γ phase to from a BCC untempered martensite structure, 2) no subsequent tempering treatment to convert the brittle UTM to pearlite or tempered martensite.

2.8 Surface Integrity in Machining

The quality of machined surface plays a prominent role in component performance, longevity, and reliability. There has always been a demand for better quality products in all applications. It is well known that machining can induce a variety of geometrical and metallurgical change in surface layers of workpiece that makes it different in nature from rest of the bulk material. When it comes to improve the quality of

machined product, the surface of product receives foremost attention. This is so because fatigue failure analyses of dynamically loaded components show that fatigue failures almost always nucleate on or near the surface of component. Various effective technologies and methods have been developed over time to improve surface quality. The term surface integrity was coined in 1964 to focus distinctly and solely on characteristics of machined or generated surfaces. Surface integrity is defined as inherent and enhanced surface condition of a surface produced in a machining or other surface generation operation [Field, 64]. It includes the existence of microcracks, untempered martensite (UTM), over tempered martensite (OTM) phase transformation, residual stresses produced by machining processes, pull out of carbides protrusions, plastic deformations, laps, craters, pits and changes in the microhardness. These factors determine the behavior and service failures of components produced. The principal causes of these surface altercations produced by machining processes are high temperatures or high temperature gradients developed in the machining process, plastic deformation and chemical reactions. The fatigue life of component is greatly affected by surface integrity, which is found to be strongly related to machining parameters. Components with improved surface integrity last longer, which justifies the cost incurred in improving surface integrity up to certain extent.

2.8.1 Residual Stresses by Hard Turning Vs Grinding

Residual stresses are unavoidable consequences of machining processes and depending upon their nature has pronounced effect on component life, creep and stress corrosion cracking resistance and component geometry. There are three main sources of

residual stresses in machining; thermal sources, micro structural transformation and deformation. The stress profile to a depth of 100-200μm is determined by the interactions of these sources and may be quite complicated. Simultaneous considerations of thermal and mechanical affects provide an understanding of their interactions. It is well understood that mechanical effects primarily result in compressive residual stresses and thermal affects primarily result in tensile residual stresses.

In machining large amount of heat may be generated at the surface work piece, part of which enters the work piece. The depth and magnitude of temperature rise of work piece surface will depend upon the amount of heat generated and upon the thermal capacity and thermal conductivity of the work piece. During machining, different layers will be heated to different temperatures the surface layer being heated more (due to proximity to the cutting tool) than the bulk material. When cooling, the surface layers cool at faster rate than bulk material. This different cooling and heating rate during thermal cycling give rise to residual stresses of complicated origin in the surface layers. Further if the temperature generated is sufficiently high, the yield strength of surface layer will be considerably reduced by the temperature to a value below that of a bulk material. However since it is thermally induced plastic deformation, which leads to residual stress, any factor, which increases this deformation, will also change the stress.

Both destructive (etching inspection and hole drilling) and non-destructive methods (X-ray diffractometry) are available for measurement of residual stress on surfaces, while former is used to determine residual stresses in surface region and later are used to determine residual stresses at surface . The most widely used technique is X-ray diffractometry. X-ray diffraction residual stress measurement is unique in that

macroscopic residual stresses can be determined nondestructively and it is able to detect stress gradients less than 5 μm below the surface. However for exact stress analysis at various dephs, it is necessary to remove successive layers of material. In X-ray diffraction residual stress measurement, the strain is measured in the crystal lattice and the residual stress producing the strain is calculated. This is based on the assumption of linear elastic theory of solid mechanics.

Matsumoto [86] studied the effect of hardness on residual stress generated in AISI 4340 steel and concluded that material hardness significantly affects the residual stress beneath the machined surface. Mechanical deformation was found to be the dominant factor which produced compressive residual stress in hardened machined surface and the effect of thermal load was considered to be secondary. Phase transformation was observed in machined surface when a tool with a worn cutting edge is used to cut hardened steel. No phase transformation occurs in machined surface if a tool with a sharp cutting edge and without any chamfer is used. It was evident that at lower workpiece hardness, the residual stress is tensile. It was shown that residual stress in soft (annealed) steel is mostly tensile stress and that in hardened steel is mostly compressive stress. Wu [90] made an effort to explain the cause of variation of residual stress with hardness by analyzing the underlying mechanism of stress formation. They concluded that for machining various hardness of work materials, the change in residual stress pattern is mainly caused by the change of shear angle in the chip formation process. Tönshoff [95] reported tensile residual stresses on the surface, machined with ceramic and CBN tools.

Many research studies have been done on the stresses induced in steel by surface grinding. In any grinding process there are numerous variables which can influence the

residual stress in the surface and sub layer of material. Some important one are the mechanical properties, structure and composition of metals, the depth of cut in grinding, feed and speed of the grinding wheel and wheel parameters and coolant used. In early 1950s, Colwell [55] studied the effect of residual stress induced by grinding hardened 4340 steel. He concluded that the higher the hardness of the steel, the higher the value of residual stress produced in the material. Also the depth of penetration of residual stress increased as the austerity of grinding increased. Halverstadt's [58] research showed that by using lower grinding wheel speeds, down feed, high work speed and a sulfurized oil coolant, he could minimize the residual stress in the material. In early 1970's Malkin [74] studied the thermal effect of grinding in the workpiece. He tried to understand how the structure changes in the material surface and sublayers due to the residual stress. He concluded the 60 percent of the total thermal energy generated in grinding flowed into the workpiece. Yonetani [84] measured the residual stress in high hardness specimens ground with various conditions. The results of his research show that the magnitude and distribution of residual stress was greatly affected by the volume change due to the tempering of the surface layer material caused by the heat generated in grinding. He also showed that the maximum residual stress and grinding temperature have a linear relation. The linear relationship depends on the hardness of each specimen. Helieby's [80] research indicates that abusive grinding produces tensile residual stress since the thermal effect becomes dominant and that gentle grinding generates compressive residual stress due to the mechanical effect. More recently, Leskovar [85] investigated and measured the residual stress on and beneath the surface after rough and fine grinding with different grinding wheels. His results show that grinding with a freshly dressed wheel produces

compressive stresses just beneath the surface, but these soon change into extremely high tensile stresses. He also showed that different types of abrasive did not affect the hardness of the surface.

2.9 White Layer

"White layer" is a generic term for a very hard material on component surfaces produced under a variety of situations, such as manufacturing processes: grinding, hard turning, reaming [Turley, 75], drilling [Field, 64, Griffiths, 85], milling [Field, 70, Koster, 70], blanking [Zener, 44], and electrical discharge machining [Field, 70, Koser, 70, Kruth, 95], service applications such as sliding [Kuritsyna, 56, Xu, 92] and rolling contact [Scott, 67, Harrison, 79], and impact [Zhang, 97]. The exact mechanism of formation of white layer has not been established yet. Three mechanisms have been suggested for the formation of white layer [Griffin, 85]. 1) Plastic flow which produces a homogeneous structure or one with a very fine grain structure. 2) Rapid heating and quenching which results in transformation products. 3) Surface reaction with the environment e.g. nitriding, carburizing and oxide ploughing. White layer is often harder and brittle than the bulk material and appears white under an optical microscope. However there is no consensus regarding many crucial properties of white layer. There are many conflicting opinions relating to microstructure, hardness, composition and formation mechanism, of white layer and their effect on product performance and fatigue life. The microstructure of white layer is also a controversial subject as it does not etch. For example, Chou [99] reported γ as high as 33% in the turned white layer compared to about 11% γ in the bulk material of AISI 52100 steel (62 HRc). In contrast, Akcan [99]

suggests that the amount of γ, if any, is much less than 10% in the white layer after turning the same material as in [Chou, 99]. Recently Barbacki [02] observed that white layer contains mainly ferrite instead of untempered martensite and austenite observed by some authors and noted the presence of austenite in deeper parts of the layer. Further, transmission electron microscopy (TEM) analysis has shown that the turned white layer consists of polycrystalline, varying in size from less than 100 nm [Barry, 02] to the range of 100 ~ 300 nm [Barbacki, 02, Akcan, 99] depending on the workpiece materials to be machined, which bears no similarity to conventional α or γ. Eda, [81] found the ground white layer was composed of fine α-phase (re-quenched martensite), ά-phase (tempered martensite), fine recrystallized γ_R phase (retained austenite) and fine secondary phases of Fe_3C, Fe_3O_4 and FeO. In light of these widely varying observations regarding microstructure of white layer, it is pertinent to mention some points about its constituent phases observed. It is well known that untempered martensite produced by various heat treatment procedures does etch with common etchants used for steel. So if white layer is untempered martensite then why is it etch resistant? Further if white layer contained retained austenite which is well known to be a soft phase, as observed in some studies, then there has to be some explanation for high hardness of white layer. Some publications postulated that presence of white layer increases the fatigue life of components [Field, 64, Tönshoff, 95], on the other hand some reported that despite white layer occurrence, hard turned steels have greater fatigue life [Abrão, 96]. Two conflicting opinions exist regarding wear resistance of surface with white layer. Griffiths [87] postulated higher wear resistance of surface having white layer. In contrast Yang [96] found wear resistance to be reduced due to presence of white layer. The significance of

the white layer during chip formation was recognized [Vyas, 00]. The white layer on the machined surface rather than in the chip is focused in this work since it is more directly related to product performance. Abrão [96] addressed the surface integrity of turned and ground surface but no white layer was obtained in ground sample probably because grinding conditions employed were extremely gentle. Recently Barbacki [02] also explained microstructural changes in surface layer of hard turned and ground samples. No through comparison of properties of white layer produced in hard turning and grinding and their effect on product performance and fatigue life of component has not been done so far. Based on literature review, white layer properties are summarized at appropriate places with respect to: Surface structure, effect of process parameters, microhardness, microstructures and chemical composition, retained austenite content, defects

2.9.1 Effect of Process Parameters

Tönshoff [95] found that the tool flank wear is a dominant factor for the white layer thickness in turning. Chou and Evans, [98] have shown that white layer thickness in turning increases with cutting speed, but may become saturated at high speeds. Further, the depth of cut has very slight effect on the white layer thickness. The effects of flank wear and cutting speeds on the white layer thickness have been confirmed in another study [Akcan, 99]. Barbacki, [02] gave the first approximation of maximum thickness of the white and dark layers in turning, as functions of cutting speed, depth of cut, and tool flank wear. In addition, cooling medium was suggested not to influence the white layer thickness but makes the dark layer thinner in hard turning. As for grinding, Tomlinson,

[91] found the white layer thickness in grinding EN. 24 steel increases as the infeed rate, the dress leads, and grinding wheel wear increases, but decreases as the grinding speed increases. Eda [81] has shown that maximum white layer thickness only occurs at certain material removal rate. In addition, a thick white layer tends to form in dry grinding rather than in wet grinding, with a decrease in grain diameter and with an increase in grinding wheel hardness.

CHAPTER 3

MICROSTRUCTURE

The microstructure of material exerts a considerable influence on its properties. Examples of surface sensitive properties are yield strength, thermal conductivity, electrical resistivity. Perhaps the most striking example of a structure sensitive property is fracture toughness, which measures the ability of a material to inhibit crack propagation and prevent brittle failure. Strength is very basic to the value of a structural material. Strength is highly dependent on microstructure because it is proportional to the difficulty of moving dislocations through the crystal lattice. Microstructure of material also influences ductility. Provided that dislocations move easily through the material and macroscopic instabilities (such as necking) do not intervene, ductility can be very large. Any microstructural element that leads to local cracking will tend to lower ductility by decreasing the load carrying capacity of the material. Inclusions, second phase particles, grain boundaries, for example, are all potential fracture sites.

Many techniques are available to determine the microstructures. By using optical microscopy, we observe shape of dendrites and grains. Fracture surface and shape of moderate-size precipitates (> 0.5mm) can be observed by scanning electron microscopy (SEM). If we need to observe smaller precipitates (~0.5 mm), or dislocation structure

after deformation, we use transmission electron microscopy (TEM). Atom-probe field ion microscopy (APFIM) allows analyzing more atomic-level chemistry such as composition of nano-scale precipitates, chemistry change at interfaces and boundaries. In this chapter white layer formed by two competing processes are characterized and compared by Optical Microscopy and Scanning Electron Microscopy (SEM).

3.1 Literature Review

A major concern in hard turning is the generation of undesirable changes to the surface microstructure and the formation of tensile residual stresses. When hardened steels are machined, high temperatures are generated along the shear plane, tool rake face and at the newly formed work surface during machining. In addition, the work material is substantially plastically deformed. A primary source of heat generation on the work surface is due to rubbing of the tool flank wear land, on the newly formed workpiece surface, added to this, the work surface is also mechanically stressed by the tool. The workpiece temperature may exceed the austenizing temperature (AC_3) in which case, the initial microstructure of the workpiece, usually tempered martensite transforms completely to austenite. The transformation may be aided by mechanical stresses and deformation imposed by the tool. The transformed layer is speculated to be untempered martensite (UTM) having a high hardness but a low fracture toughness. Often, this surface layer appears as a white featureless layer in optical micrographs. The microstructure of the layer has been suggested to be untempered martensite and retained austenite though this has not been definitely established. The layer is often referred to as the white layer (WL) because the microstructure does not react with the etchants typically

used to bring out the microstructure of steels and therefore appears white when observed under the optical microscope. White layers are similar to grinder burns and they are undesirable since the untempered martensite is extremely brittle. Typically an overtempered layer forms under the white layer due to the material being heated up to temperatures below the AC_3 temperature, which produces a tempering effect. This layer is softer compared to the white layer as well as the bulk of the workpiece material due to overtempering. Understanding the microstructure is vital in determining material properties such as strength and ductility.

3.1.1 Surface Structure

It is generally agreed that if austenitizing temperature is exceeded in machining, rapid self-cooling can produce a white layer on the machined surface. A hard-turned surface with white layer usually consists of three layers [Tönshoff, 95, Chou, 98, Akcan, 99, Guo, 03]: a white layer (untempered martensite), a dark layer (overtempered martensite), and the bulk material. Similar surface structure was also found in a ground surface except that the dark layer is not visible if the white layer is less than 1 μm. The transition profile between the dark and white layers is in-phase with the feed rate modulation [Chou, 98]. While the transition profile is almost straight in case of a ground surface. The significant difference is the thickness of a white layer or a dark layer, which is usually below 12 μm [Toenshoff, 95, Chou, 98, Akcan, 99] in hard turning with large flank wear. The white layer thickness varies from 0 to 2 μm and the heat affected zone (white and dark layers) from 0 to 7 μm in gentle grinding [Barbacki, 02], but may be as large as 23 μm in abusive grinding [Field, 70, Eda, 81]. Additionally, a hard-turned white

layer is etch resistant and shows featureless structure in an optical image. It is not clear that if a grinding-induced white layer is also etch resistant.

3.1.2 Microstructure

The white layer was often referred as recast [Stier, 88] or re-hardened layer [Toenshoff, 95]. While Matsumoto [84] and Vyas [00] claimed that the white layer has a mixed untempered martensite (α) and austenite (γ). The volume fractions of α and γ in a white layer have been controversial subject discussions in a number of papers. For example, Chou [99] reported γ as high as 33% in the turned white layer compared to about 11% γ in the bulk material of AISI 52100 steel (62 HRc). In contrast, Akcan [99] suggests that the amount of γ, if any, is much less than 10% in the white layer after turning the same material as in Chou, [99]. Barry, [02] indicated that the volume fraction of γ in a turned white layer increases with increased flank wear, but no austensite reflections were found on the white layer surface, rather, the presence of γ was recorded in deeper parts of the layer. Recently Barbacki [02] observed that white layer (at least in hardened 1%C, 1.5%Cr steel) contains mainly highly dislocated micro and nanograins of ferrite instead of untempered martensite and austenite observed by some authors. He also noticed that white layer consists mainly of micrograins of α- phase and no austenite was noticed in superficial part of white layer, but the presence of austenite was recorded in deeper parts of the layer. He stated that cooling medium does not influence the white layer thickness but makes the dark layer thinner in hard turning. Further, transmission electron microscopy (TEM) analysis has shown that the turned white layer consists of polycrystalline, varying in size from less than 100 nm [Barry, 02] to the range of 100 ~

300 nm [Barbacki, 02, Akcan, 99] depending on the workpiece materials to be machined, which bears no similarity to conventional α or γ. Dynamic recovery was thought to produce such nanograins in a turned white layer. As for grinding, Eda, [81] found the ground white layer was composed of fine α-phase (re-quenched martensite), $\acute{\alpha}$-phase (tempered martensite), fine recrystallized γ_R phase (retained austenite) and fine secondary phases of Fe_3C, Fe_3O_4 and FeO. The dark layer was composed of $\acute{\alpha}$-phase, precipitated Fe_3C phase, γ_R- phases (partially transformed into bainites) and sorbite structure.

3.2 Experimental Procedures

AISI 52100 cold finished, spheriodized and annealed 26.98 mm diameter bars of Brinell hardness 183 were cut into two groups of test samples. AISI 52100 steel is widely used in hard machining and therefore used as the test material in this study. To ensure test data repeatability, ten turning samples and ten grinding samples were prepared. Each turning sample is 177.80 mm in length and 26.98 mm in diameter, and each grinding sample is a short cylinder of 12.70 mm high and 26.98 mm in diameter. Before heat treatment to the required hardness, the grinding samples were gently ground to make the sample thickness uniform. This step is essential to ensure generating uniform white layer in a ground sample. The chemical composition of the work material as specified by the manufacturer is listed in Table 3.1. The properties of AISI 52100 bearing steel are given in Table 3.2

Table 3.1 Nominal Chemical Composition (% by weight) of AISI 52100 Steel

C	Mn	P	S	Si	Ni	Cr	Mo
1.02	0.34	0.009	0.005	0.28	0.06	1.52	0.02
Al	Cu	V	Ti	N		O	
0.024	0.05	0.005	0.002	0.0065		0.0006	

Table 3.2 Properties of ANSI 52100 bearing steel

Young's Modulus (GPa)	Density P (kg/m^3)	Yield Strength (MPa)	Thermal Conductivity At 100°C (W/mK)	Specific Heat C (J/KgK)	Austenitizing temperature (°C)
201	7833	1410	43	550	775-800

All the turning and grinding samples were austenized at temperature of 1500 F for two hours, quenched in oil at 150 F for 15 minutes, then tempered at 350 F for two hours. The measured average hardness (external surface and inside across the diameter) for each sample is 63.08 HRc with a standard deviation of 0.28.

In order to compare white layer properties by hard turning and grinding, thick white layers have to be produced for reliable measurement. Extensive literature review on the effects of process parameters on white layer thickness were conducted to reduce the time spending on trial and error methods. Dry turning tests were conducted on a high precision EzPath II Romi-Bridgeport CNC lathe Figure 3.1. A worn CBN insert of 0.1 mm initial flank wear instead of a fresh one was used to facilitate generating thick white layer. The process parameters, Table 3.3, were selected to generate a thick white layer. After cutting two passes of 150 mm long each, the tool was withdrawn from cutting, and then flank wear was found to be 0.6 mm. Then a test sample of 12 mm long

corresponding to the flank wear was sectioned from each turned bar using EDM. The tuned samples were polished at both ends to remove the EDM affected layer. Dry grinding was performed on a manual grinding machine Figure 3.2 with a worn grinding wheel. The applied grinding parameters were also listed in Table 3.3. The literature review [Eda, 81, Tomlinson, 91] has shown that the maximum thickness of a white layer occurs at a certain material removal rate. We therefore selected two grinding conditions, condition A for possible maximum white layer thickness, while condition B for verifying the effect of material removal rate on the white layer thickness. The grinding wheel ground the workpiece in one pass during each test.

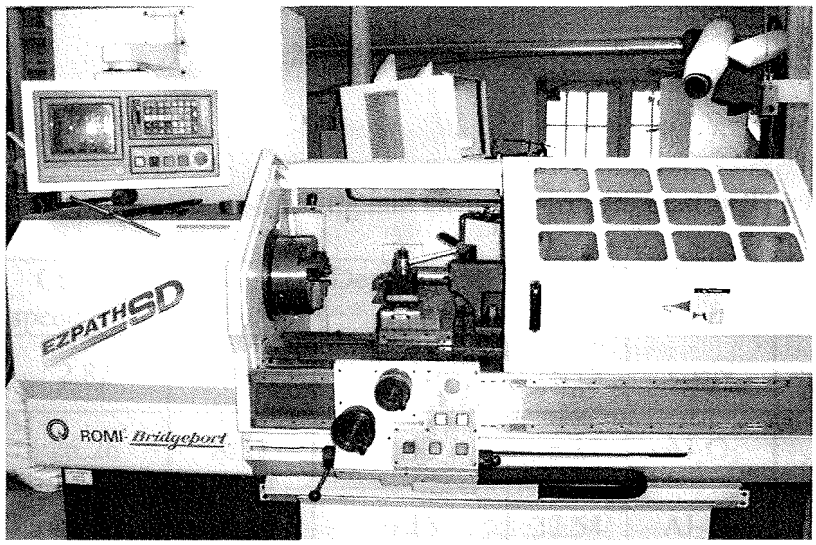

Figure 3.1 Romi-Bridgeport EzPath II CNC lathe

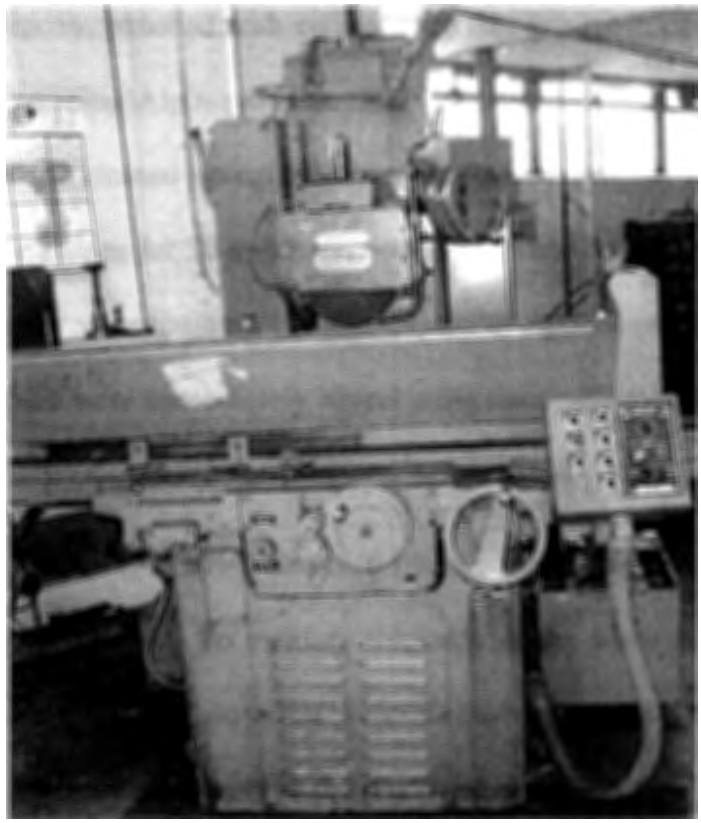

Figure 3.2 Manual Surface Grinder

Table 3.3 Process Parameters of Turning and Grinding for Generating Thick White Layer

Operation	Cutting speed (m/s)	Feed rate (mm/s)	Depth of cut (mm)	MRR (mm^3/s)	Tool Materials	Work Material
Turning	2.82	1.66	0.20	28.15	CBN	AISI 52100 (62~63 HRc)
Grinding A	26.26	8.33	0.13	16.27	Al_2O_3	AISI 52100 (62~63 HRc)
Grinding B	26.26	16.66	0.13	32.54	Al_2O_3	AISI 52100 (62~63 HRc)

3.3 Sample Preparation

The white layers induced in hard turning and grinding were analyzed using optical microscopy, scanning electron microscopy (SEM). Samples were sectioned with an abrasive cutter, mounted in a cold-setting epoxy with the machined surface portion

exposed from the epoxy, polished with successively fine grit mesh of 180, 240, 400 and 600 followed by polishing Al_2O_3 paste on 0.03 μm polishing paper until a mirror-like surface was obtained, cleaned using lab detergent and dipped in acetone solvent to perform ultrasonic cleaning for 30 to 45 seconds, then etched for about 10 seconds using 2% nital solution for observation of white layers in optical microscopy and SEM analyses. The samples were immediately rinsed using running water and dried using hot air.

Surface structure: An Olympus BH-2 binocular phase contrast microscope Figure 3.3 was used to study surface structure. To measure thickness of the white and dark layers, the white layer and the surrounding materials were contrasted under the optical microscope to differentiate microstructure changes in the machined layer.

Figure 3.3 Olympus BH-2 Optical Microscope

Microstructures: A Philips XL 30 Scanning Electron Microscope was used to study the microstructure Figure 3.4. The SEM is equipped with an Energy Dispersive Spectrometer (EDS) and has both back-scattered electron and secondary electron detectors for imaging. The SEM is operated through a PC based system. SEM pictures of the surface structure (white and dark layers) after turning and grinding and the work material before machining were taken to compare the microstructure changes at different magnifications. The samples were mounted on the specimen holder and transferred into the SEM chamber. High vacuum (pump) was created in the SEM chamber. Accelerating voltage of 20 kV was used in the SEM analysis.

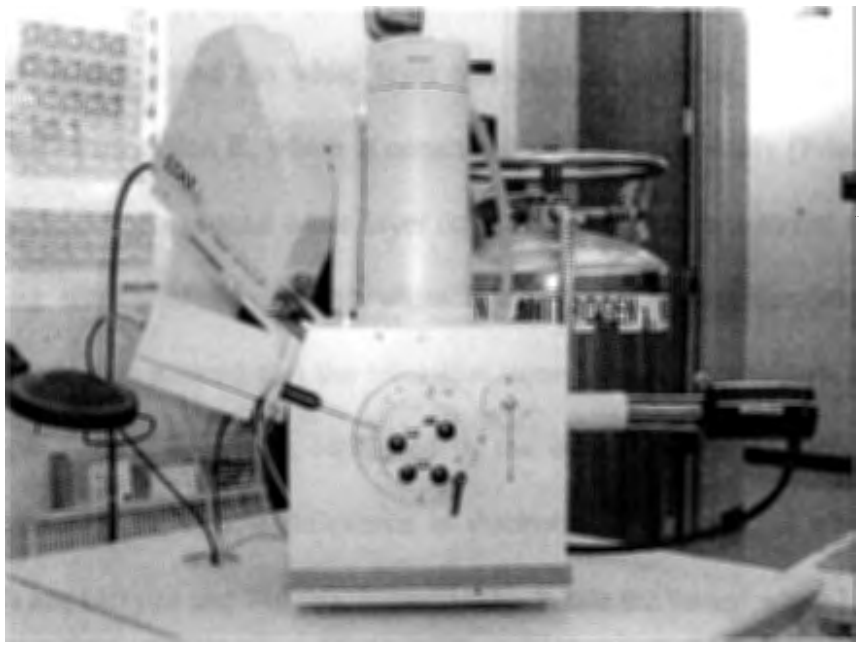

Figure 3.4 Philips XL 30 Scanning Electron Microscope.

3.4 Results and Discussion

3.4.1 Surface Structure

Figure 3.5 shows surface structure of the hard turned samples under the turning conditions in Table 3.3. The 14.1 μm thick white layer, then 34.4 μm dark layer (including the white/dark layer transition zone), followed by the bulk material appears in the cross section of all the turned samples. The transitions zones between the white/dark layers and the dark layer/bulk material are also noticeable. The corresponding tool flank wear for this turned surface structure is 0.6 mm. The generated white layer thickness is thicker than those reported by several studies [Barbacki, 02, Tönshoff, 95, Chou, 98, Akcan, 99], which allows more reliable microhardness measurement since the white layer thickness is much larger than the indent size. Similar surface structure of the ground samples, i.e., the white layer, the dark layer, followed by the bulk material, also appears in Figure 3.6. It was found the white layer thickness in grinding condition A is 21% larger than that in condition B, which is consistent with an early study [Eda, 81] that the maximum thickness of a ground white layer only occurs at certain material removal rate. The following results of the ground white layer refer grinding condition A unless otherwise stated. It is noticed that the transition zone between white/dark layers of the ground sample cannot be clearly identified in the optical image. Compared with the turned samples, the significant difference is thickness of the ground white and dark layers, which are 140 μm and 740 μm, respectively. While the turned white layer is rarely above 15 μm even using a worn tool with flank wear much larger than 0.6 mm. One may infer that high grinding temperatures penetrate deeper into the workpiece, resulting in a

thick ground white layer. Therefore, abusive grinding tends to produce a much thicker white layer than abusive turning.

It was found that the transition zone between the white/dark layers in the turned samples and ground samples is very different, Figures 3.7 and 3.8. A transition zone between the white/dark layers can be identified but not clear in the turned sample at a high magnification. However, the transition zone of the ground sample is very clear and looks very different from the turned sample. Only partial ground white layer was shown in Figure 3.8 in order to show the white/dark layer transition zone. The thickness ratio of the dark layer to the white layer is 2.44:1 for the turned sample and 5.29:1 for the ground one, which could be explained that the development of a dark layer is largely suppressed in hard turning due to the stress-induced hardening of the workpiece material as a result of Hertizan stress [König, 93]. It should be pointed out that the so-called "white" layer under an optical microscope doesn't appear "white" anymore in a SEM picture. Rather the turned white layer appears more dense and uniform than the dark and bulk materials, but the ground white layer doesn't.

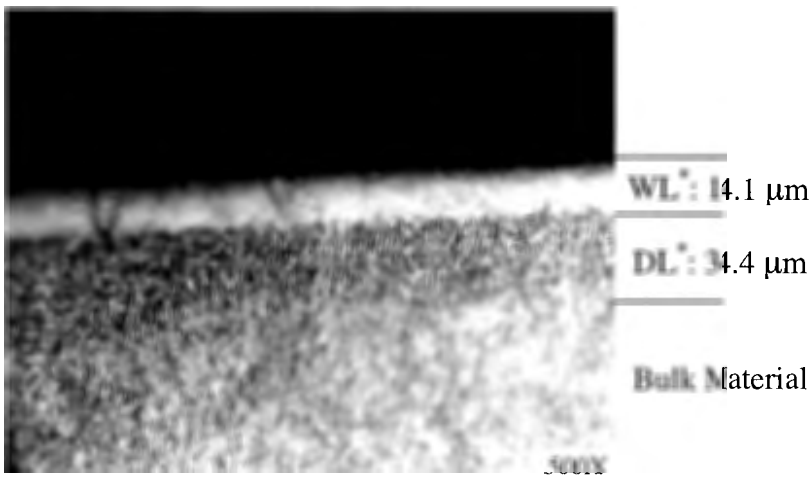

Figure 3.5 Surface Structure of the Hard Turned Samples
(V: 2.82 m/s, f: 1.66 mm/s, DoC: 0.2 mm, VB: 0.6mm)
* WL: white layer, DL: dark layer.

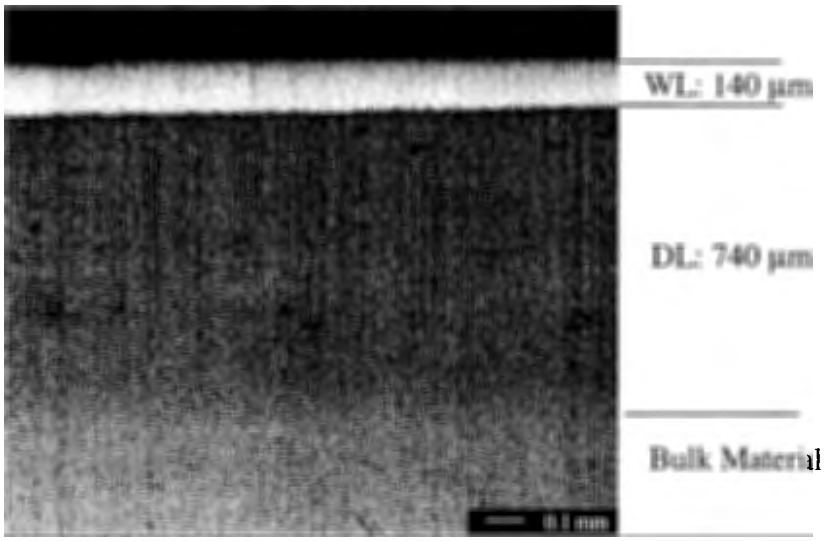

Figure 3.6 Surface Structure of the Ground Samples
(V: 28.26 m/s, f: 8.33 mm/s, DoC: 0.13 mm, worn grinding wheel)

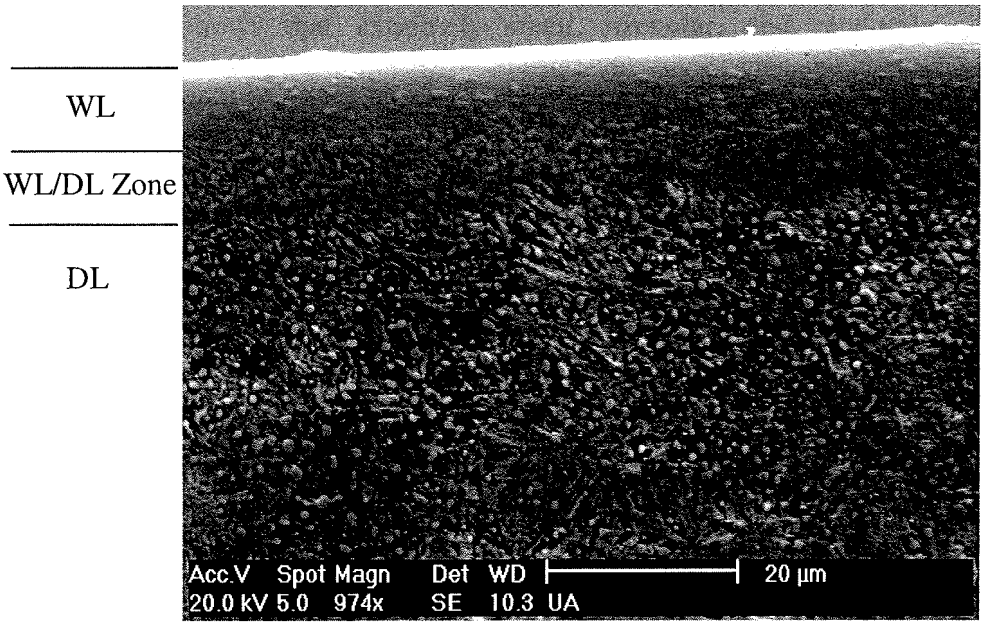

Figure 3.7 SEM Surface Structure of the Hard Turned Samples

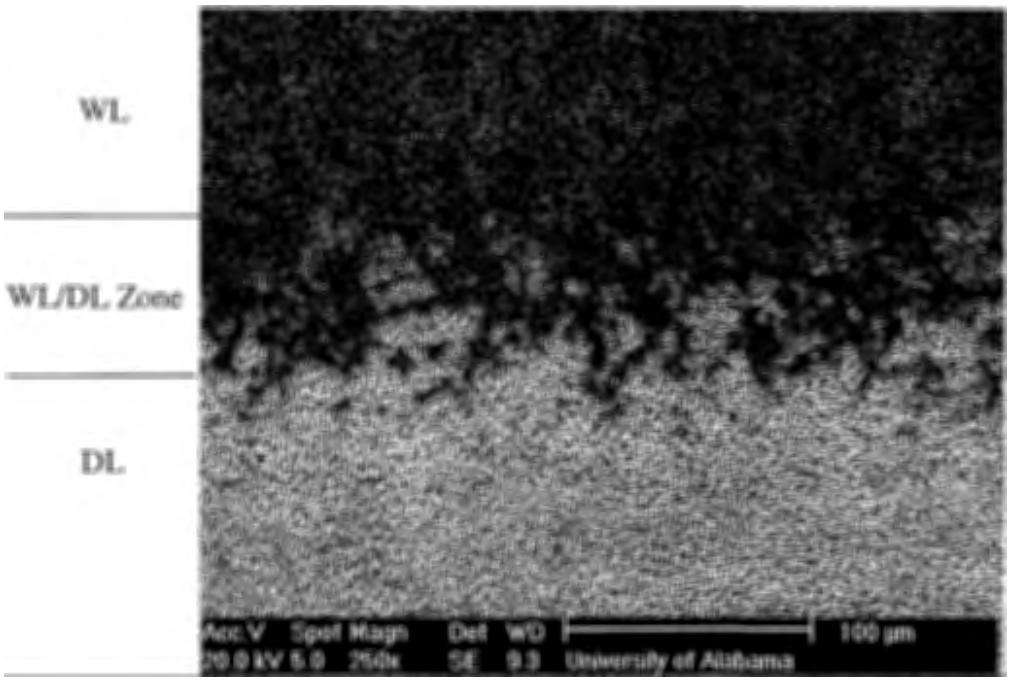

Figure 3.8 SEM Surface Structure of the Ground Samples

3.4.2 Microstructure

Figure 3.9 shows that extremely small, irregular, and randomly dispersed cementite particles are embedded within a continuous ferrite matrix in the bulk material before machining. The turned white layer seems to be severely strained in the cutting direction and the random cementite particles buried in the ferrite matrix material, Figure 3.10(a). The turned white layer is etch resistant so that the SEM picture shows a featureless structure. Etch resistance of the turned white layer may be attributed to its nanograins of 100 ~ 300 nm in size [Barbacki, 02, Akcan, 99, Barry, 02] resulting from dynamic recovery and recrystallization. Trent [2000] pointed out that the dynamic recovery process accompanies dislocation movement, resulting in the formation of very small equi-axed grains and many new boundaries, which make the flow zone etch resistant. In contrast, Figure 3.10(b) shows clear microstructures of the turned dark layer.

The ferrite matrix was greatly etched and the cementite particles retain their original shape and distributions. The etched dark layer explains why it is most soft compared with the white layer and bulk materials.

The significant difference between the turned white layer and the ground one is that the ground white layer is etched and therefore its microstructures are clear, Figure 3.11(a). It should be pointed out that same etching procedure was used in preparing the turned and ground specimens. In the ground white layer, the ferrite matrix was etched and the cementite particles retain their original shapes and distributions instead of severely strained in the cutting direction in a turned white layer. Though the ground white layer is etched, its microstructures are still different from those of the bulk material as shown in Figure 3.11. Compared with the tuned dark layer, the ground one is much more severely etched, which is clearly seen from the ferrite matrix structure, Figure 3.11(b). It explains why the ground dark layer is softest across the ground surface and is softer than that of the turned dark layer. In addition, the cementite particles protrude from the etched matrix material in the ground dark layer. Besides surface structure characteristics and microhardess profile, this is another important aspect illustrating that different mechanisms may be activated in generating the turned and ground white layers.

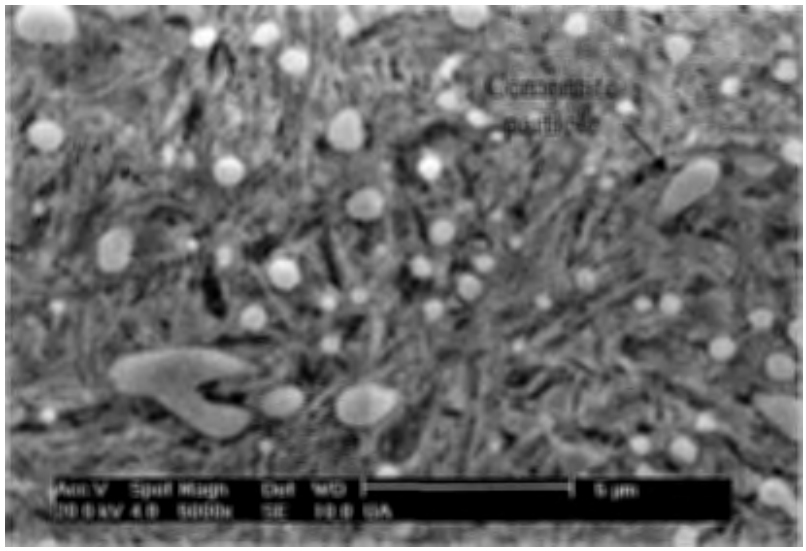

Figure 3.9 Microstructures of the Bulk Material by SEM before Machining

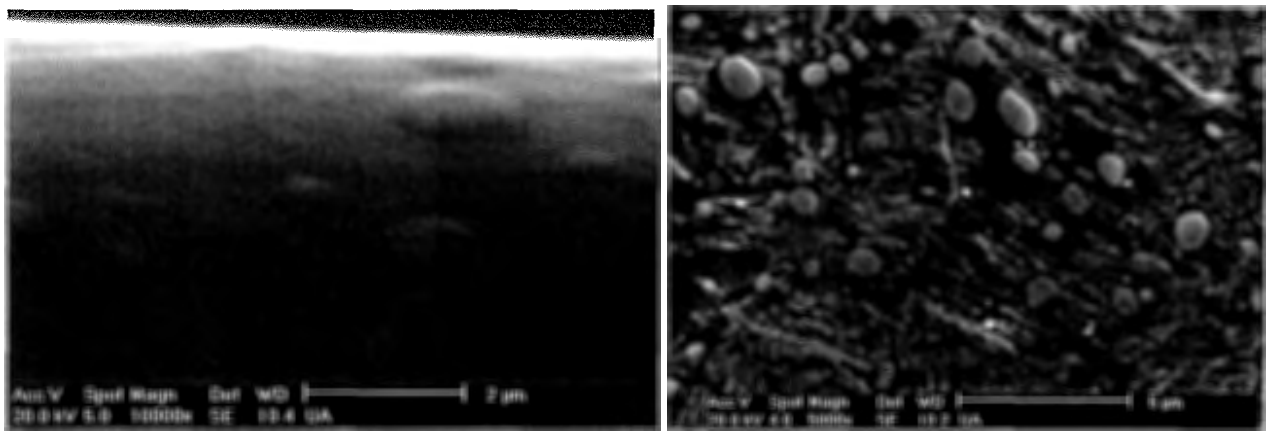

(a) White Layer (b) Dark Layer

Figure 3.10 Microstructures of the White and Dark Layers by Hard Turning

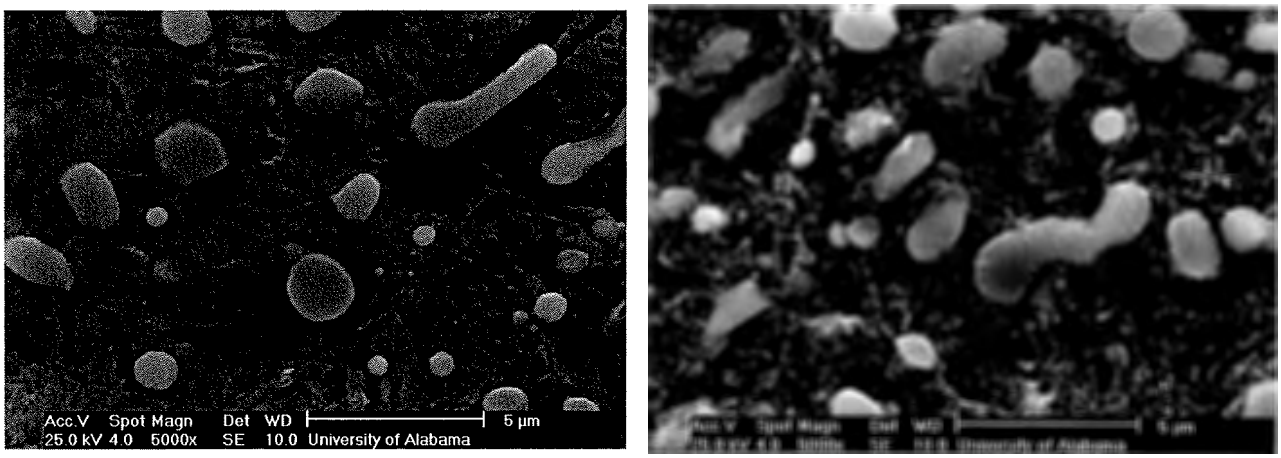

(a) White Layer (b) Dark Layer

Figure 3.11 Microstructures of the White and Dark Layers by Grinding

CHAPTER 4

MICROHARDNESS

Hardness is the property of material to resist plastic deformation when subject to contact action on its surface. Hardness measurement has found exceptionally wide application in the quality control of metals and metal components, owing to the rapidity and simplicity of the tests, as well as possibility of accessing the properties of a material without destroying the component. Various microhardness tests have been developed for applications where it is necessary to determine the hardness of a very small area of material or where the material or modified layer is very thin. A typical microhardness tester used to measure microhardness is shown in Figure 4.1. A pyramidical diamond indenter having an angle of 136° between opposite faces and 146° between opposite edges is pressed into the surface of the metal under a load of W kg and the mean diagonal d (mm) of the resultant indentation is measured. The Vickers hardness number is practically independent of load which is applied for a period of usually 15 seconds. The Vickers hardness number is determined by Equation 4.1 [Tabor, 00]:

$$V.D.H. = \frac{0.9272W}{A} \tag{4.1}$$

A is the projected area of indentation. The value is expressed in Kg/mm^2

The relation between the Vickers hardness and mean yield pressure over the indentation (P_m) is given by Equation 4.2.

$$V.D.H. = 0.9272P_m \tag{4.2}$$

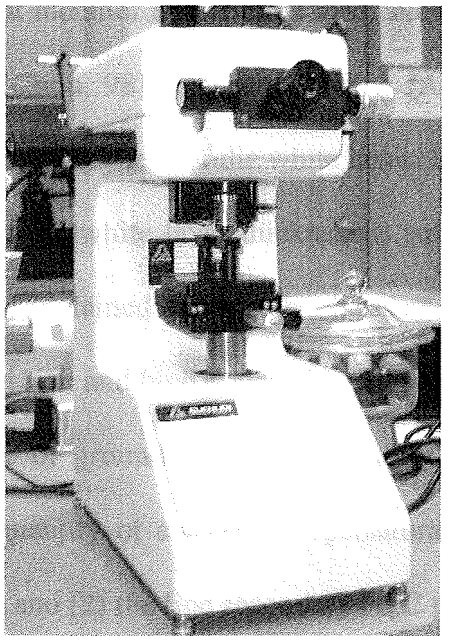

Figure 4.1 . Rockwell Hardness Tester

4.1 Literature Review

The Microhardness test is very useful in identifying metallurgical changes such as white and dark layers at various depths below the machined surface. However many a times microhardness readings are misleading due to small size of altered subsurface layers or overlapping of layers and often large unexpected variation in microhardness values are noticed. A number of studies have shown those white layers are characterized by increased hardness whereas the dark layer shows decreased hardness in turning [Guo, 03; Barbacki, 02; Töenshoff, 95; Akcan, 99; Vyas, 00]. In contrast [Chou, 99]

showed that the white layer in hard turning AISI 52100 steel (59-61 HRc) is approximately the same hardness in average as the bulk material white the dark layer is substantially softened. The reported variation of microhardness data [Chou, 98] is reasonable due to feed mark modulation and the embedded hard particles in soft matrix. It has been noticed that different indenter and applied load, such as 25g [Töenshoff, 95] 40g [Barbacki, 02], and 100g [Chou, 98], and nano-loading [Akcan, 99], were used in these measurements with different thickness of the white layer. It is obvious that reliable measurement is only possible if the white layer thickness is sufficiently larger than the indent size. [Barbacki, et al., 02] explained that high hardness of a turned white layer was caused by extremely small grain size and high dislocation density. While [Eda, et al., 81] attributed the hardness increase of ground white layer mainly to (1) fine untempered martensite containing a great quantity of carbon in supersaturated state in the base α-phase (re-quenched martensite), and (2) the fine secondary Fe_3C phase precipitates.

4.2 Experimental Procedure for Microhardness

For Turning: The thickness of turned white layer as measured from optical micrograph was 14.1μm in our experiments and the size of indentation was about 8μm. So for reliable measurements, a taper magnification technique was used for turned samples. This technique increases the apparent depth of different layer and enables more and reliable readings of microhardness to be taken. Also careful experiments were conducted to ensure that whole indentation falls in the white layer. The sample was sectioned from the turned specimen using abrasive wheel cutter. The cut sample was mounted in epoxy with machined surface on the top. The sample was polished using standard metallographic

procedure as described in section 3.3. The final dimensions of turned specimen are shown in Figure 4.2. A literature review reveals that previous studies for micorhardness testing used etching to expose the white layer on polished surface. It was thought that etching may effect the hardness of different layers. To study the variation of microhardnes along depth of a machined surface and to effect of etching on microhardness reading, six sets of experiments were conducted for microhardness testing. The hard turned and ground white layer samples were tested before and after etching. After polishing, the surface was etched slightly so that various layers are clearly visible under the optical microscope.

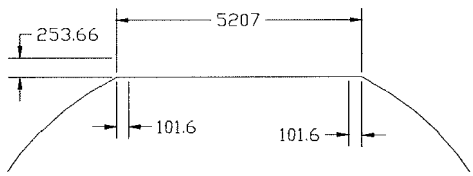

Figure 4.2 Final specimen after taper sectioning

Actual thickness of white layer	: 12 μm
Depth of polishing	: 253.66 μm
Exposed surface width after polishing	: 5207 μm
White layer width after polishing	: 101.6 μm
Magnification	: 101.6/12 = 8.4

For Grinding: The grinding samples were polished and etched using metallographic specimen preparation procedure described in section 3.3. No taper sectioning was needed

because the thickness of phase transformed layers was large enough (as noticed in optical micrograph) for reliable hardness measurements to be made.

For Untempered sample: The hardness of untempered material was also tested before and after etching.

4.3 Results and Discussion

Figure 4.3, 4.4 and 4.5 shows the hardness profile below the surface. Hardness variation is expected since the randomly distributed hard cementite particles, Figures 4.7-4.11, affect indent size and thus hardness readings. Also usually small size of the phase transformed layer in machining necessitates the use of low load for microhardness test. At low load there is always an error associated in measuring the length of diagonal of small indentation. It is obvious that the characteristics of microhardness profiles for hard turned and ground samples are similar, in which microhardness in white layer is much higher then that in dark layer and bulk material and microhardness of dark layer is slightly lower than that of bulk material. It demonstrates that both types of white layer have the highest hardness due to microstructure changes. This observation is consistent with previous studies [Guo, 03; Barbacki, 02; Tönshoff, 95; Akcan, 99; Vyas, 00].

The exact value of microhardness of turned and ground white layer cannot be predicted with certainty due to fluctuations observed in hardness readings. The significant difference is that the hardness of ground white layer is about 10 % higher than tuned one, but the ground dark layer is softer than the turned one.

It was found that etching affects the hardness of 52100 steel as more fluctuations are observed in microhardness reading in etched samples as compare to polished only

samples. Furthermore, etching seems to affect only the matrix of bulk material and to some extent the dark layer, but not white layer as hardness pattern in white layer before and after etching seems to be same or the variation is not detectable in this study. Contrary to expectations, the hardness of untemperated samples was found to be elevated after etching, the reason for which is not understood.

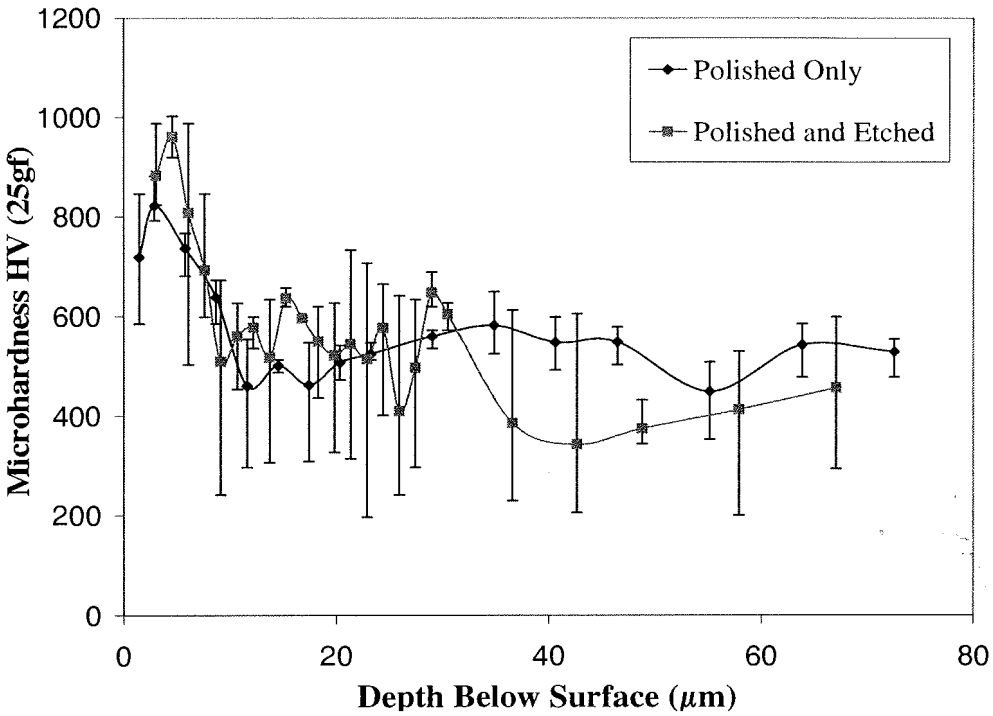

Figure 4.3 Microhardness of Turned Sample

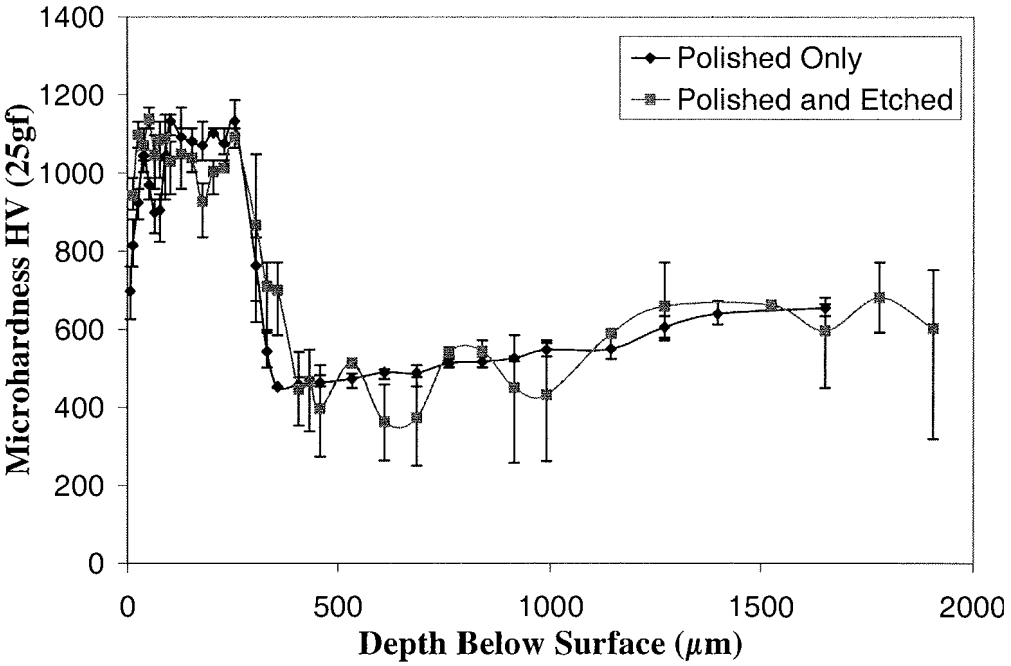

Figure 4.4 Microhardness of Ground Sample

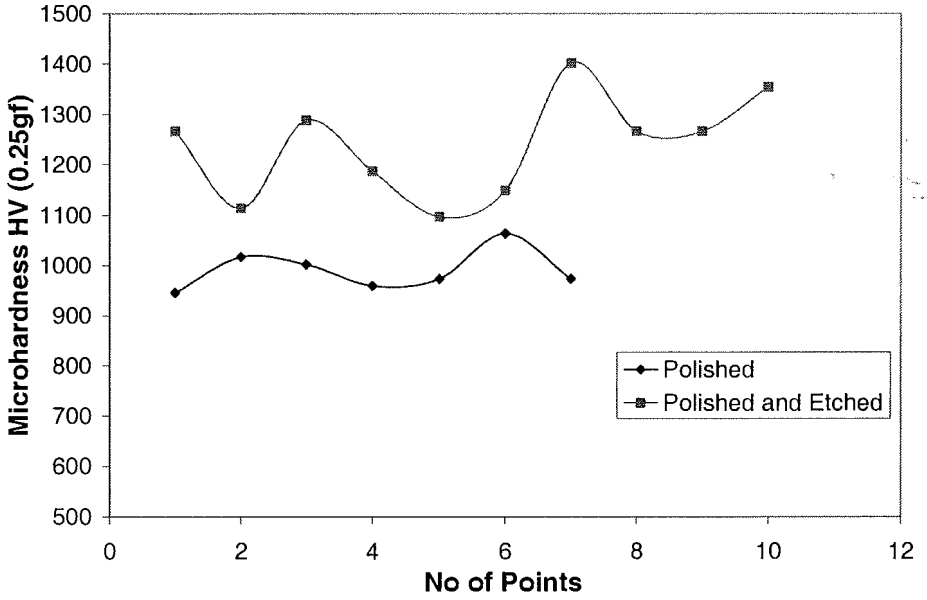

Figure 4.5 Microhardness of Untempered Sample

CHAPTER 5

CHEMICAL COMPOSITION

The machined surface experiences high temperature followed by immediate quenching by surrounding air. It is believed that during this rapid thermal cycle, significant elemental changes may occur at the surface of the machined part. In this chapter hard and turned white layers are analyzed using XPS (X-ray photo spectroscopy) to detect any elemental changes that may have occurred due to severe thermal cycle induced in machining.

5.1 Literature Review

The elements (Mn, Cr, Si, and S) were found distributed evenly against the distance from the surface, except carbon (C) concentration increases slightly in the turned white and dark layers [Tönshoff, 95]. As for the ground white layers, Eda [81] found that in the vicinity of the ground white layer, sulphur and phosphor show a decrease in concentration, while manganese and carbon show an increase in concentration. What is noteworthy in the results obtained so far is a rise in the concentration of carbon in the ground white layer.

5.2 Experimental Procedure

The XPS analysis was done on Kratos AXIS 165 Multitechnique Electron Spectrometer Figure 5.1. AXIS 165 is equipped with both standard dual (Mg/Al) anode and monochromatic (Al) X-ray sources for XPS analysis and imaging, a 15 keV electron gun for AES analysis and Auger or secondary electron imaging, and a 5 keV ion gun for sputter depth profile, sample surface cleaning and sputter deposition. The electron energy analyzer is a 165 mm mean radius concentric hemispherical analyzer equipped with 8 channeltron detectors. Instrument control, data acquisition and data analysis are performed through the Kratos Vision 1.5 software operating on a Sun Sparc Station IV platform. An x-ray source of a monochromatic Al K_α line was used to determine the chemical composition of the turned and ground white layers and the bulk material before machining. The applied excitation energy, width, gun current, gun voltage, and pass energy were 1486.6 eV, 1 eV, 0.02 amps, 15000 V, and 80 eV, respectively. XPS analysis was conducted immediately after sample finish polishing, washing, and drying to prevent surface oxidation. The samples were prepared by standard metallographic procedure as discussed earlier during study of microstructure. After mounting, the samples on the specimen holder were put into the surface transfer chamber (STC) in which vacuum was created. Then the samples were transferred to surface analysis chamber (SAC). Ultra high vacuum (10^{-9} – 10^{-10} torr) was created in SAC. The laser beam was focused on the sample surface whose chemical composition is to be determined.

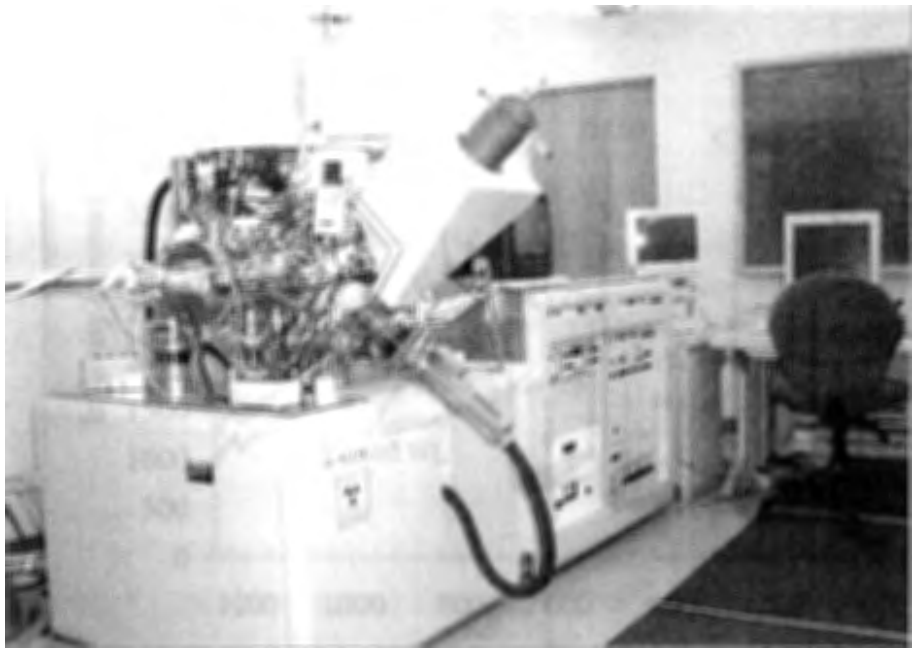

Figure 5.1 Kratos AXIS 165 Electron Spectrometer

5.3 Results and Discussion

Broad scan survey spectra, Figure 5.2, for the bulk material, the turned white layer, and the ground white layer were obtained to identify the interested elements of present. The used Al K_α x-ray allows the photos have a limited penetrating power in a solid on the order of 1-10 nm, which allows chemical composition analysis of the white layers in this study. Obviously, the C (1s), O (1s), C (KLL), and O (KLL) lines are prominent in the spectra, while the signals of other elements (Mn, P, S, Si, and Cr) are weak. By comparing the test data with the standard spectra of the elements [Moulder, 95], it was found that both the turned and ground white layers are rich in oxygen, which indicates that the work materials reacts with the environment and results in oxides.

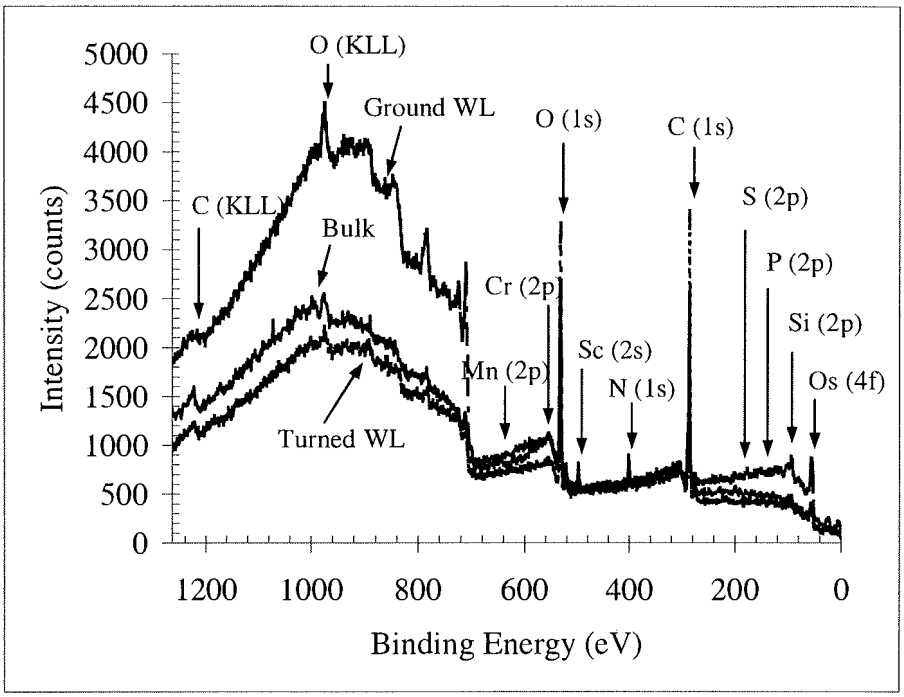

Figure 5.2 XPS Survey Spectra of the Bulk Material and White Layers (WL)

Spectrum, Figure 5.3, for each individual element (C, O, Mn, P, S, Si, and Cr) of interest was also obtained to determine the relative element concentration. Based on the intensity, i.e., the number of detected electron, the relative element concentrations of the turned and ground white layers are summarized, Table 5.1, compared with the bulk material. The variations of Carbon (C) and Oxygen (O) in the turned and ground white layers are opposite, which may be attributed to different white layer formation mechanisms. For example, grinding temperature and time duration in the workpiece are much larger than those of hard turning, therefore, the interaction between the workpiece and the environment would be fundamentally different from the scenario of a turned part. High grinding temperature and long time duration will promote chemical reaction between the workpiece and the environment, and result in oxides in the ground white

layer. The mechanisms of variations of other elements are complex and will be further studied in the future.

Table 5.1 Relative Element Concentrations in the White Layers (WL) Compared with the Bulk Material*

Category	C	O	Mn	P	S	Si	Cr
Turned WL	+	–	––	+	+	–	–
Ground WL	–	+	–	++	+	+	#

*+: increase; ++: more increase; –: decrease; ––: more decrease; #: no change

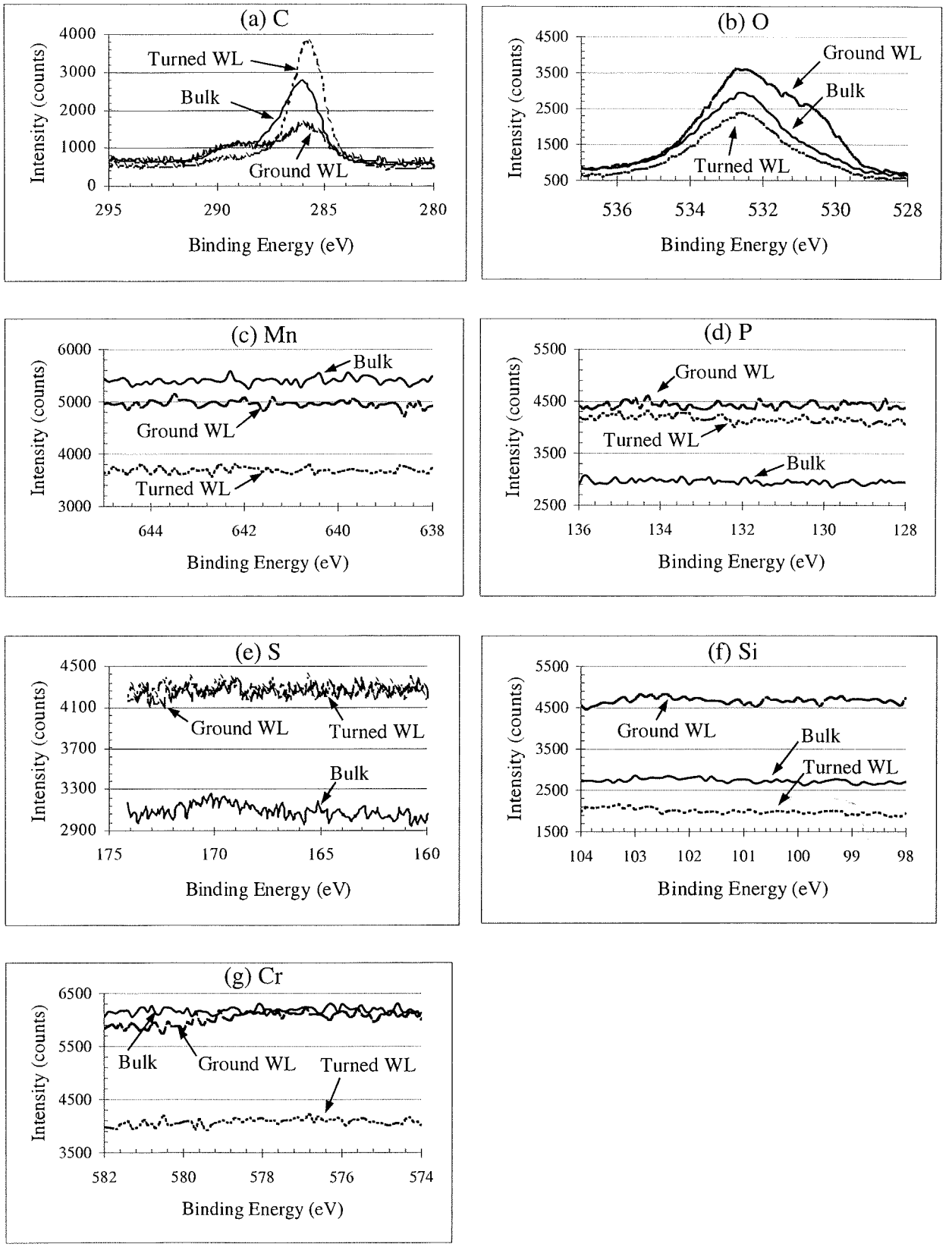

Figure 5.3 XPS Spectrum of Individual Elements in Bulk Material and White Layer

CHAPTER 6

X-RAY DIFFRACTION ANALYSIS

Retained austenite is usually formed in steel during the heat treatment of steel. During the hardening process, the steel is heated to high temperature followed by quenching and tempering process. During this heating cycle, steel is transformed into austenite which is subsequently transformed to hard and brittle martensite by rapid quenching. However the phase transformation during quenching is not as ideal as this. Often some of the austenite is retained in martensite structure depending upon the rate of quenching, percentage of carbon and alloying content of steel. The higher the carbon and alloying element content of steel and the lower the points M_s and M_f, the more of austenite will be retained. When there is appreciable amount of retained austenite in martensite, it can be observed in the microstructure as bright fields between the martensite needles or as interlath films in quenched carbon steels. The purpose of this study is to determine the volume percentage of retained austenite in AISI 52100 steel before and after machining in the machined subsurface layers. The volume fractions of retained austenite were measured before and after machining in base material, turned white layer, turned dark layer, ground white layer and ground dark layer.

6.1 Significance of Retained Austenite in Steel

Retained austenite is known to have both positive and negative effects on properties of the machined surface.

6.1.1 Disadvantage

The presence of retained austenite in the machined surface is considered a defect since it is known to degrade the surface quality. Retained austenite can transform to martensite during service due to thermal and mechanical stresses encountered. Martensite has a BCC unit cell structure, which is slightly larger than the FCC unit cell structure of austenite. This can severely affect the dimensional stability of the precision components which can cause seizure of moving components. This causes unnecessary inconvenience and additional costs of maintenance and replacement. Apart from that it is known to lower the aggregate compressive yield and ultimate strengths and thereby load carrying capacity of martensitic/austenitic structures. Also it lowers the hardness and resistance to scuffing and indentation and increases susceptibility to burn and heat checking in machining operation [Jatczak, 80].

6.1.2 Advantages

On the other hand some advantages of presence of retained austenite in steel have been reported. Results from experiments work carried out by Zhu [85] on a rolling contact fatigue testing machine with two rollers as specimens showed the contact fatigue resistance of the specimen with the largest amount of retained austenite is much better than with smaller amount of retained austenite. Yokoi [96] carried out the investigation of the effects of strengthening mechanisms on the fatigue properties of high strength steels. The results indicated that the compressive residual stress caused by transformation from

retained austenite to martensite under the cyclic load can retard the propagation of the microcracks.

Opposite opinion exists regarding the affect of retained austenite on the mechanical behavior of steel. The role of retained austenite on fracture toughness remains controversial [Haidemenopoulos, 89]. For example toughness improvements have been reported with presence of retained austenite in 4340 steel. In contrast other studies indicate a decrease in toughness in the second stage of tempering attributed to austenite decomposition. Haidemenpoulos [89] postulated that retained austenite has little effect on toughness of steel. It improves contact fatigue life in gears and bearings made from carburizing and homogeneous high carbon steels.

6.2 Retained Austenite in White Layer

This investigation is motivated by relatively different opinions on effect of retained austenite on part fatigue life as material as discussed in section 6.1 and widely different observations regarding the volume percentage of retained austenite in turned and ground white layer. For example, Chou [99] reported γ as high as 33% in the turned white layer compared to about 11% γ in the bulk material of AISI 52100 steel (62 HRc). In contrast, Akcan [99] suggests that the amount of retained austenite, if any, is less than 10% in the white layer after turning. Barry [02] indicated that the volume fraction of γ in a turned white layer increases with increased flank wear, but no austensite reflections were found on the white layer surface, rather, the presence of γ was recorded in deeper parts of the layer.

6.3 Background

The measurement of volume fraction of retained austenite can be made from X-ray diffraction. X ray diffraction method is considered to be the most effective method to determine volume fraction of retained austenite in steel. The volume fraction of retained austenite in steel is determined by comparing the integrated chromium or molybdenum X-ray diffraction intensity of ferrite and austenite phases with theoretical intensities. A chromium X-ray source was used in this study. Chromium radiation produces minimum florescence in iron and it provides for the needed X-ray diffraction peak resolution and allows for the separation of carbide peaks from austenite and ferrite peaks. Copper source of X-rays produces too much fluorescence and obscures the diffraction peaks. In this study, it is assumed that the material has a nearly random crystallographic orientation and has few undissolved carbides.

6.4 Experimental Procedure

Sample Preparation: Six samples were prepared by the regular metallographic procedure as discussed in section 4.3 to measure and compare the volume fraction of retained austenite in steel. The six samples analyzed were:

A) Turned white layer

B) Turned dark layer

C) Ground white layer

D) Ground dark layer

E) Untempered bulk material

F) Bulk material

For sake convenience, the above nomenclature may be used in this study to refer to different specimens.

The phase identification for the samples was carried out on the Philips MPD 3040 diffractometer with CrKα radiation. Filler was used to reduce the intensity of the K_β line which may appear in final XRD scan. The specimens were analyzed with 2θ values in the range of 60° to 110°.

6.5 Results and Discussion

The steel matrix is considered to consist of two phases, α-ferrite or γ-retained austenite. Then the constituent phases can be represented by Eq (6.1).

$$V_M + V_A = 1 = 100\ \% \tag{6.1}$$

V_A and V_M are the volume fraction of austenite and martensite respectively in the sample. The volume fraction of carbides was ignored. Quantitative determination of the relative volume fraction of ferrite and retained austenite in each sample can be obtained from XRD pattern obtained because the X-ray intensity diffracted from each phase is proportional to volume fraction of that phase. The integrated intensities, instead of maximum intensities were used in analysis in order to avoid variations that may be introduced by grain size, micro strain, etc. The volume fraction of retained austenite is calculated from the following equation (6.2):

$$V_A = \frac{I_A/R_A}{I_A/R_A + I_M/R_M} \tag{6.2}$$

The integrated intensity, I_A and I_M from each sample were measured from the corresponding diffraction pattern whereas volume fraction of retained austenite, R_A and

R_M were calculated from the basic principle as discussed in SP-453 information manual by XRD division of SAE. The planes selected for diffraction were (200).

The X-ray diffraction patterns from all six samples are shown in Figure 6.1. Retained austenite is non trivial in steels (like 52100) with significant carbide fractions and martensite. All the diffraction patterns exhibit high intensity peaks corresponding to the α-ferrite phase. The XRD diffraction pattern of the hardened and tempered bulk material exhibits α-ferrite peaks at about 68.9^o and 106^o. In contrast, the diffraction pattern of untempered specimen exhibits a possible γ-austenite peak at about 79^o along with some sharp carbide peaks which indicates the presence of austenite. This observation suggests that the tempering process involves dissolution of carbide in ferrite phase. The austenite peaks are less evident in tempered and untempered materials as compared to other XRD patterns. This is in agreement with the final volume fraction of retained austenite calculated in samples E and F.

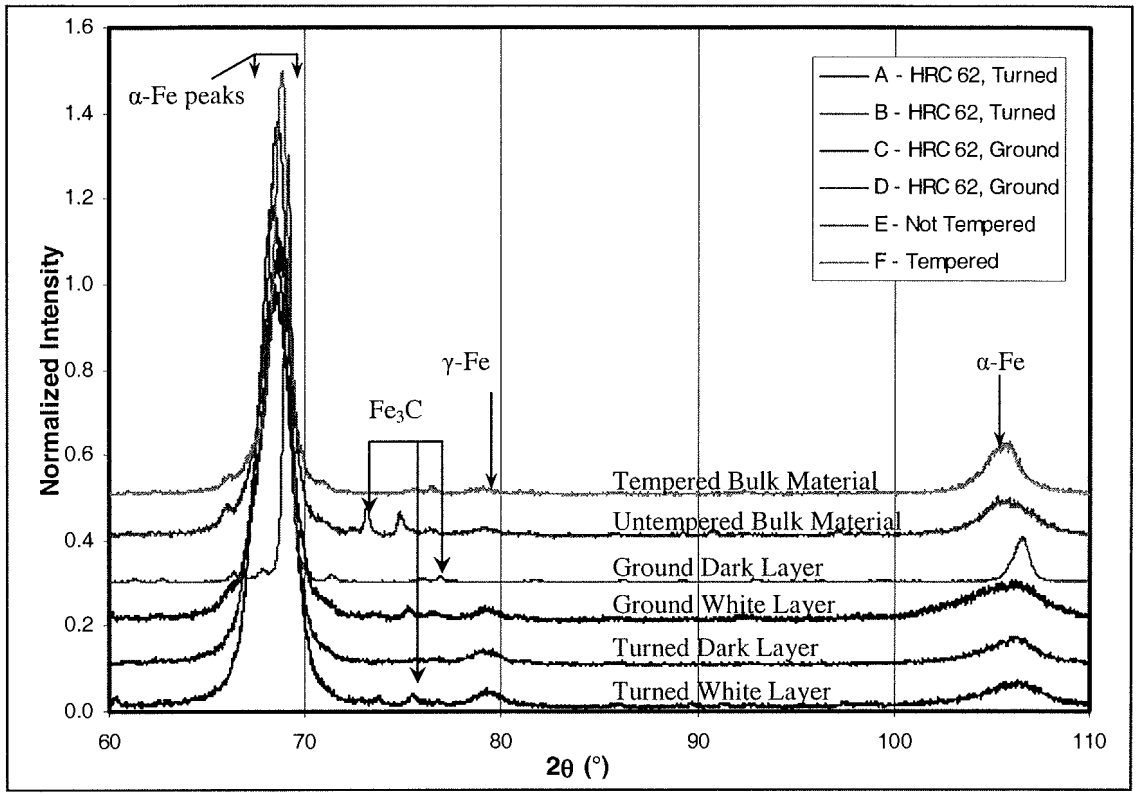

Figure 6.1 X-Ray Diffraction Pattern of all Samples using CrKα radiation

The XRD pattern of turned and ground dark layers is clearly different. The XRD pattern of ground dark layer also exhibits some peaks due to ferrite phase at about 69 and 107°. But the ferrite peaks of ground dark layer are comparatively narrow as compared to ferrite peaks of other samples. It is clear that sample C experienced more heat during grinding than did sample D. Some carbide peaks are also visible. Strangely, the sharp carbide peaks are diminished, and the possible retained austenite peak is very small or absent. The reason for this unexpected variation in XRD diffraction pattern of ground dark layer from the other patterns is not clear at present. In contrast, no carbide peaks are evident from scan of the turned dark layer. The observation is supported by the calculated percentage of retained austenite in two dark layers. The turned dark layer has 14.6% γ-

phase as compared to 0% observed in ground dark layer Table 1. It is worthy to note that the percentage of retained austenite observed in turned dark layer is more than in ground dark layer.

The diffraction pattern of the turned and ground white layers looks very much similar. Both depict likely retained austenite peaks and some carbide peaks. But the calculation indicates that percentage of retained austenite in turned white layer (13.3%) is much more as compared to that in ground white layer (3.6%). This estimation is known to be first ever comparison of retained austenite content in turned and ground white layer.

Table 6.1 Volume Fraction of Retained Austenite

Sample Name	Intensity Austenite (200)	"R" Austenite (200)	Intensity Ferrite (200)	"R" Ferrite (200)	Volume Fraction Austenite
A	22.8	34.78	88.9	20.73	13.3%
B	31	34.78	107.9	20.73	14.6%
C	10.5	34.78	165.7	20.73	3.6%
D	0	34.78	215.7	20.73	0.0%
E	13.4	34.78	151.5	20.73	5.0%
F	13.1	34.78	175.6	20.73	4.3%

6.6 Conclusions

Samples A, B, C, D, E, and F are martensite in various degrees of tempering. Based on peak widths, the order from most tempered to least tempered is D, F, E, A, B, C, with A and B being about the same. If this interpretation is correct, sample D experienced enough heat during grinding to temper, but not enough heat to form austenite or quench rate to form martensite. The variation in low intensity sharp peaks is not clear yet. The increased width of samples A, B, and C may also be due to plastic deformation.

CHAPTER 7

TEM ANALYSIS

7.1 Introduction

It is well known that microstructure determines the material properties. Transmission electron microscopy (TEM) is a versatile tool for studying crystal structures, lattice parameters, grain size and lattice defects (dislocations, glides, twinning etc). One of the advantage of TEM analysis over other methods is that it uses electron for examining the material and the wavelength of electrons is much smaller than that of light. Also the resolution attainable for TEM images is many orders of magnitude better than that from a light microscope. Thus, TEM can reveal the finest details of internal structure - as small as individual atoms even.

7.2 Literature Review

As discussed earlier, XRD studies have revealed the variations of retained austenite in white layers produced by hard turning and grinding. The TEM study of white layer was undertaken to compare and understand white layer in hard turned and ground surfaces. This will help to clear the ambiguity regarding the phases and microstructures of white layers. In an earlier TEM study [Turley, 75] of structure of white layer formed

on reamed hole, sufficient evidence of the presence of carbides was found in electron micrographs and diffraction patterns. But a general loss of carbides in white layer was noticed on comparison with bulk material. It was suggested that some of the carbides were annihilated by the dispersion of carbon to dislocation, vacancies and subgrain boundaries. Turley [75] found no evidence of retained austenite in white layer produced by reaming and grinding. Further the white layer formed by abusive grinding was observed to have a fine grained structure. It is pertinent to mention that structures of white layer formed by abusive grinding and reaming were found to be different.

7.3 Specimen Preparation Procedure

Two types of samples are in use for TEM:

1) Planar section
2) Cross sectional

In this study planar sections are used.

In TEM specimen preparation for planar section, the main objective is to produce a thin enough section of the material which is transparent to the electron beam inside the microscope. The first step is preparing a 3mm diameter disc of thickness of 100 to 150μm. The 3mm diameter specimen size is necessary because a standard TEM specimen holder accepts disc shaped samples of 3mm in diameter. To prepare 3mm diameter specimen, firstly the material was cut parallel to machined surface, to make a slice of about 0.5 to 1 mm thickness using a diamond disc cutter. Then a 3mm diameter section of material was cut out of slices. This 3mm diameter and roughly 0.5 to 1 mm thick disc was further ground and polished to final thickness of about 100μm. Grinding and

polishing were carried out using a variety of equipment and techniques, however in principle they are all based on material removed at the surface by an abrasive medium. One surface of the ground disc was polished to obtain a perfect surface finish condition prior to grinding a depression of controlled size, known as "dimple" on the opposite face. The term "dimpling" refers to the procedure wherein an accurately sized depression is cut on the surface of a specimen to reduce the time required for final thinning process. The instrument for this application is a high precision grinding machine composed of a turn table and a grinding wheel in mutually perpendicular planes of rotation. The grinding wheel cut a spherical depression at the centre of the disc specimen which mounts concentric with respect to the turn table platen. The system is equipped with the vertically positioned micrometer which monitors the depth of the dimple. The final product is 3mm diameter parallel sided disc of material with an approximate thickness of 100μm. The disc was dimpled to reduce the thickness at center to about 20 – 30μm.

The last step in specimen preparation, prior to its mounting and study inside the electron microscope, involves a thinning procedure to generate electron transparent areas on the mechanically pre-thinned disc specimen. The simple grinding procedure such as dimpling is not capable of reducing thickness so as to make it electron transparent. Ion milling or milling or electro polishing was used. During ion milling, ions of inert gas, Ar were accelerated in potential field and hit the specimen surface with shallow angle of incidence, thereby removing atoms form the bulk and thus reducing the overall thickness.

The prepared specimen was placed in special TEM specimen holder. The specimen holder was inserted in evacuated TEM chamber for study. This procedure was repeated to make four samples, one each for turned white layer, ground white layer,

hardened and tempered bulk material and hardened and untempered material. The specimens were examined in a Hatachi 8000-200 kV Transmission Electron Microscope Figure 7.1. The TEM has scanning capabilities for STEM work. It is also equipped with a NORAN Energy Dispersive Spectrometer (EDS) for X-ray analysis, and has a secondary electron detector for imaging. X-ray signals can also be used for X-ray mapping. The specimens were examined in both transmission and diffraction mode using accelerating voltage of 200 kV.

Figure 7.1 Hatachi 8000-200 kV Transmission Electron Microscope

7.4 Results and Discussion

7.4.1 Bulk Material:

Figure 7.2a shows a typical bright field TEM image of the microstructure of starting material. It exhibits a ledge like granular morphology which is typical of bainite (non laminar non cooperative but competitive ledge like granular) structure. In this microstructure, cementite phase was found to be present in two different morphologies; lamellar and precipitates. The lamellar form of cementite (one of such is marked as L in the micrograph of Figure 7.1) exhibits the following orientation relationships with ferrite:

$$[100]_{Cm} // [011]_{\alpha} \text{ and } (001)_{Cm} // (211)_{\alpha}$$

The orientation relationship conforms to those reported by Zhang, [97] between pearlite, ferrite and cementite. The diffraction pattern from hardened and tempered bulk material Figure 7.2b shows this orientation relationship between lamellar cementite and pearlite. The diffraction pattern taken from the sample seldom reveals that the sample was well annealed and recrystallized. That, the pattern also exhibits no distinct diffraction spots and rings due to the γ phase suggests the existence of a very small amount of retained austenite if any in bulk material. This is evident in the diffraction pattern of Figure 7.2b. Less twinning is visible in the undeformed material which is usual, since heat treatment generally produces recrystallized grains itself. Practically no visible signs of strain were noticed in the TEM micrographs taken from this sample because of the recrystallized condition of material.

The precipitate form of cementite, one of which is shown by an arrow in Figure 7.1, appears to exhibit more or less incoherent interfaces with the ferrite matrix and shows very little evidence of strain indicating that the material is well crystalline due to

tempering that occurred during the preparation of the starting material. This form of cementite is distributed randomly throughout the microstructure. The size of these precipitates appears to range between μm.

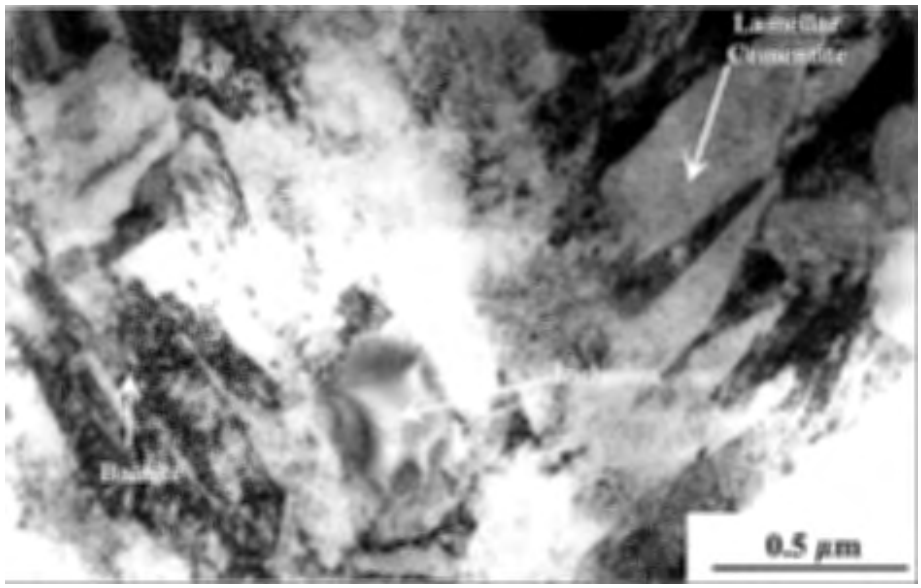

Figure 7.2a. TEM Micrograph of Undeformed Bulk Material.

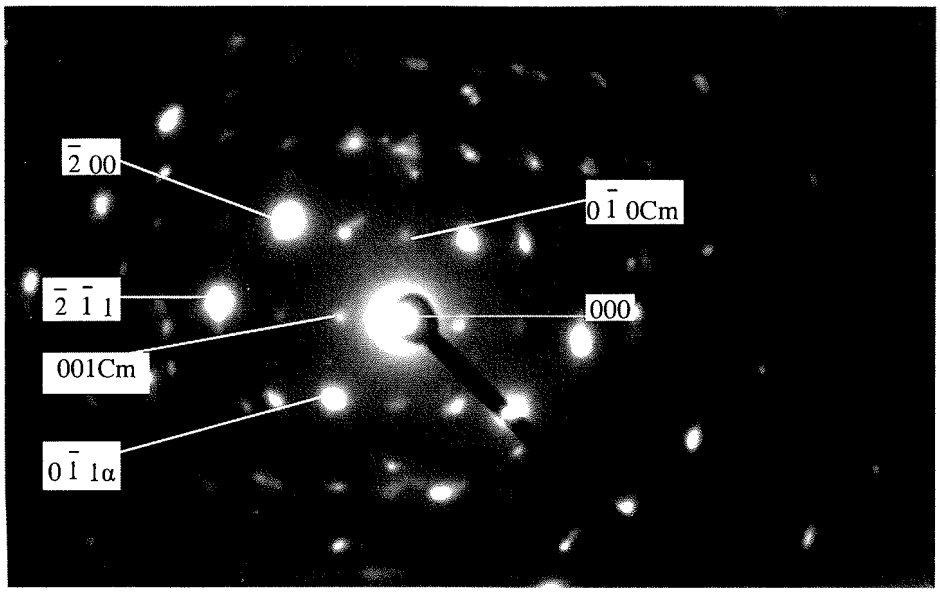

Figure 7.2b. Selected area diffraction pattern of bulk material with electron beam parallel to [011] of defective ferrite and [001] of lamellar cementite.

7.4.2 Turned White Layer:

Figure 7.3a shows typical TEM micrograph taken from the turned white layer. Inspection of this micrograph reveals that the microstructure of turned white layer is different from that of bulk material shown in Figure 7.2a. The microstructure of this sample has a lath like granular morphology with a large number of defect bands. The defect bands present in the image are similar to those observed for twins in a typical ferrous martensite. So it would be stated that during machining, the samples passed through a very high to a very low temperature quenching which had resulted in these deformation bands. The quenching thermal history just described has its support in the morphology of cementite precipitate found in the matrix of this sample. These

precipitates do not show any evidence of massive fracturing and defects that are typical of what is observed in materials undergoing heavy cold working. Figure 7.3b shows a diffraction pattern taken from the defect bands in Figure 7.3a. In the pattern, diffraction spots due to α-iron phase were indexed. Other spots in the pattern are due to defects and could not be indexed, but are expected to be martensite twins. The structure of martensite is inherently strained because of thermodynamically non equilibrium conditions under which it forms. Hence the presence of deformation bands indicates a non equilibrium thermal history, which the samples experienced during quenching. This indicates that all the cementite precipitates present in the sample were formed during recrystallization that occurred following quenching during machining from high temperature to a low temperature. Figure 7.4a and 7.4b are the TEM micrograph and the corresponding composite diffraction pattern taken from cementite precipitate and matrix. Electron beam was parallel to the [100] of the cementite crystal. The presence of fracture free cementite precipitate in the sample clearly indicates that it was formed during recrystallization that occurred following the quenching of the sample. A careful examination of the micrograph also reveals the presence of strain contrast at the precipitate and matrix interface. This strain is believed to be developed when precipitation occurs at a highly strained matrix. The matrix was highly strained due to a massive diffusionless transformation caused by quenching. The diffraction pattern of the interface reveals no orientation relationships between precipitate and the matrix. This seems to indicate that the strain at the precipitate/matrix interface is not due to co-operative mismatching of lattices across the interface. Rather it occurred during precipitation in a highly strained matrix, caused by a massive diffusionless transformation during quenching. The strain

contrast due to bending is also clearly visible inside the precipitate. Figure 7.5 is a composite diffraction pattern taken from the matrix. Diffraction rings due to α (martensite) in the pattern are indexed, but additional rings due to γ-phase are present in the pattern. Also several spots in diffraction pattern from white layer may not be indexed conclusively. Some feature of TEM micrographs are not easily interpreted due to the deformation caused by plastic deformation.

An interesting feature of the present TEM study of this sample is the observation of high precipitate density compared to that in undeformed sample. This feature of precipitates in turned white layer suggests the presence of more nucleation sites for cementite than in turned white layer which in turn may be dependent on inherent characteristics of hard turning process.

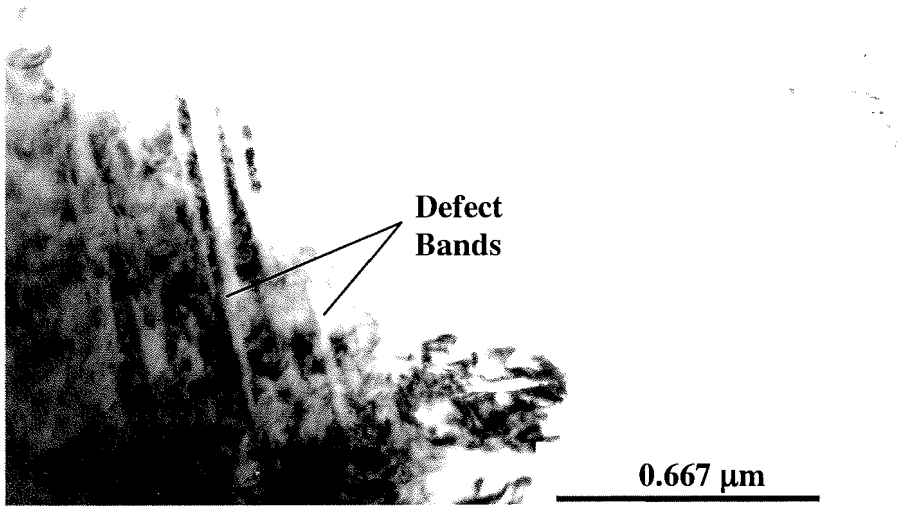

Figure 7.3a TEM Micrograph Identifying Defect Bands in Turned White Layer.

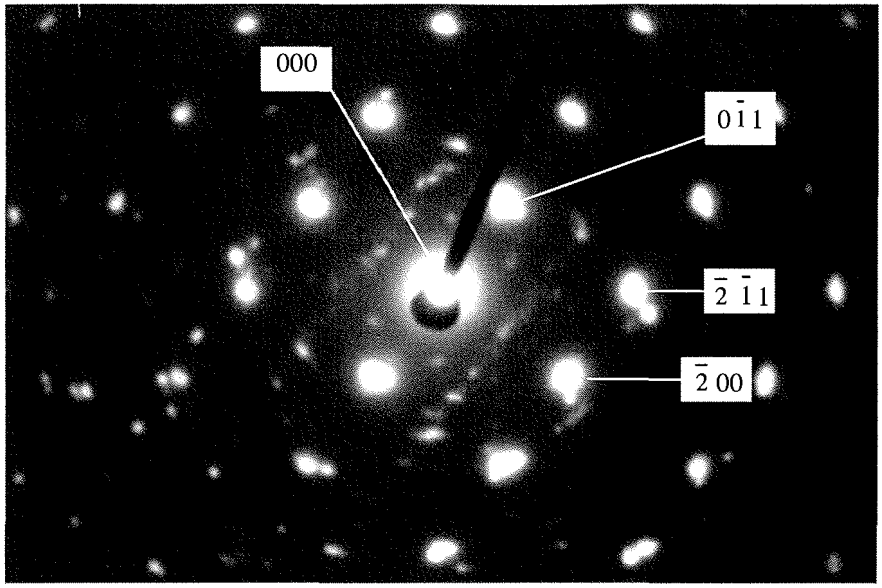

Figure 7.3b. Diffraction pattern from sample of turned white layer defective ferrite. Electron beam was parallel to [011] direction of defective ferrite phase.

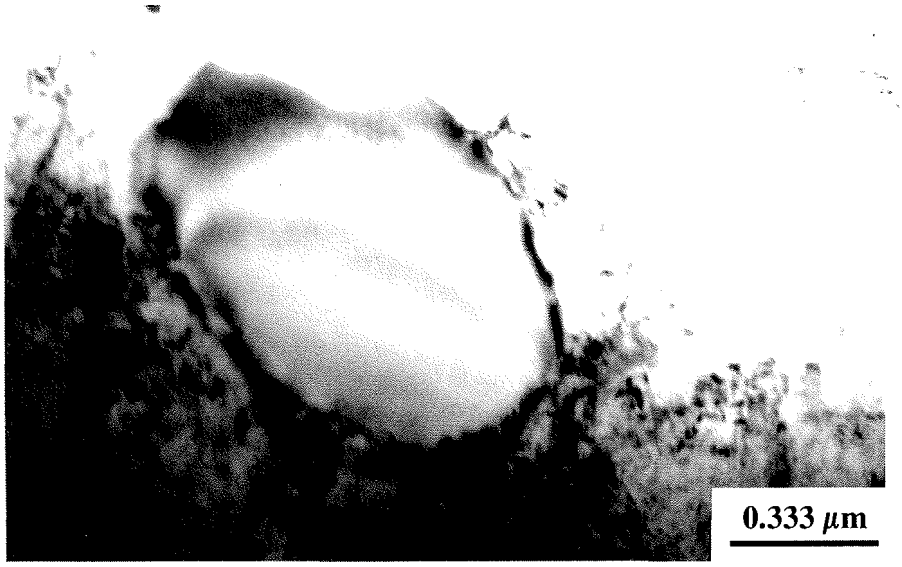

Figure 7.4a. TEM micrograph of precipitate in turned white layer

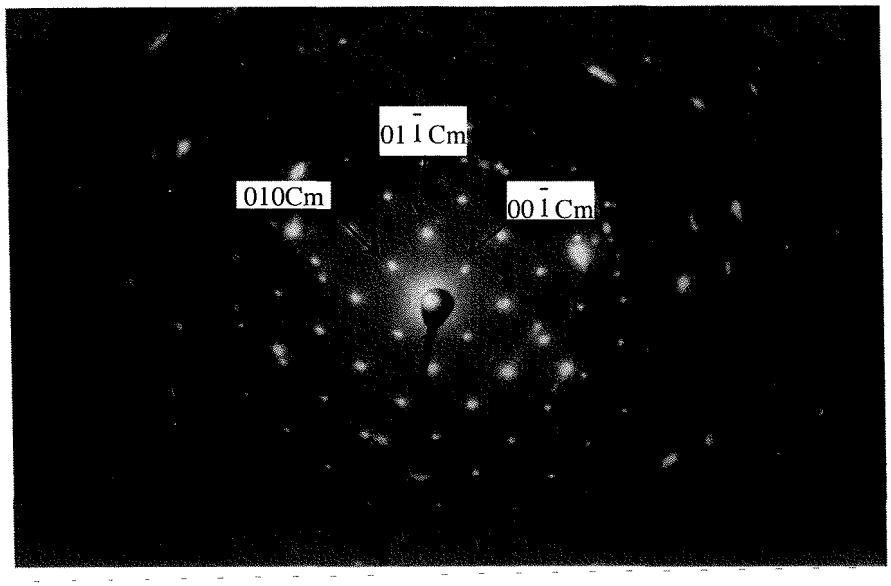

Figure 7.4b. Diffraction pattern from precipitate in turned white layer showing no orientation relationship between cementite precipitate and matrix.

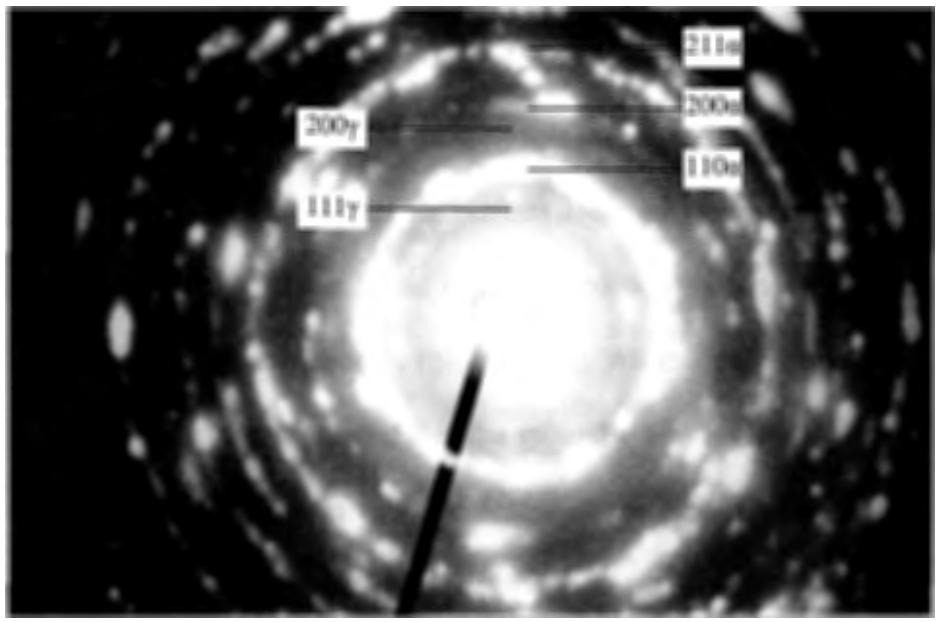

Figure 7.5 Polycrystalline diffraction pattern showing presence of retained austenite in turned white layer.

7.4.3 Ground White Layer

Figure 7.6a shows a typical micrograph taken from the ground white layer. It also exhibits defect bands similar to those observed in turned white layer sample. However the simple comparison of the two micrographs reveals that the ground white layer not only has finer but also more number of defect bands. Under the TEM any arbitrary part of thin foil specimen taken from this sample exhibited defect bands only, when the place of existing defect bands was aligned parallel to the incident beam. Even though at any arbitrary orientation of electron beam, the specimen showed a lath like plate like matrix and some defects bands. A composite diffraction pattern taken from the defect bands is shown in Figure 7.6b, which indicates that these defect bands in this sample are twin bands that are typical of those found in ferrous marteniste. Based upon this crystallographic characteristic, it was assumed that the matrix of this sample is martensite. Other notable microstructure feature found in the sample is the presence of cementite precipitates. Figure 7.7 shows a micrograph taken from this sample exhibiting such precipitates. The cementite precipitates in this samples were relatively smaller in size and larger in number than those found in the turned white layer samples. Here the precipitates also exhibited no evidence of cold working. All the microstructural features of this sample discussed so far suggested that the ground white layer was also produced by a thermal phenomenon analogous to those described for turned white layer samples i.e. fast quenching. However finer quality of deformation twins of this sample seems to indicate a maximum violent nature of quenching then that of the turned sample.

The diffraction pattern of Figure 7.6b also revealed diffraction rings due to austenite indicating that the sample contains a minute amount of retained austenite. Comparison of the intensity of diffraction rings observed in these samples, revealed the presence of more retained austenite in this sample than that of turned white layer.

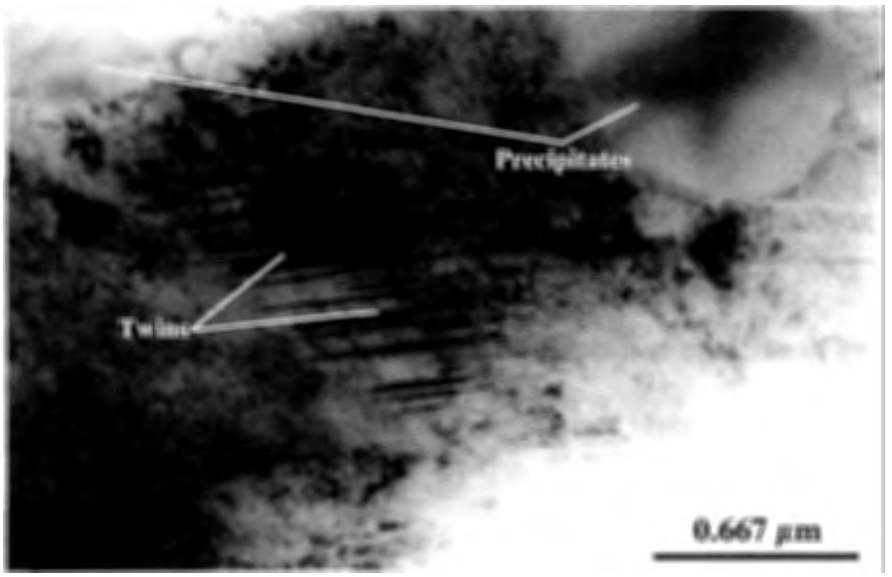

Figure 7.6a TEM micrograph of ground white layer

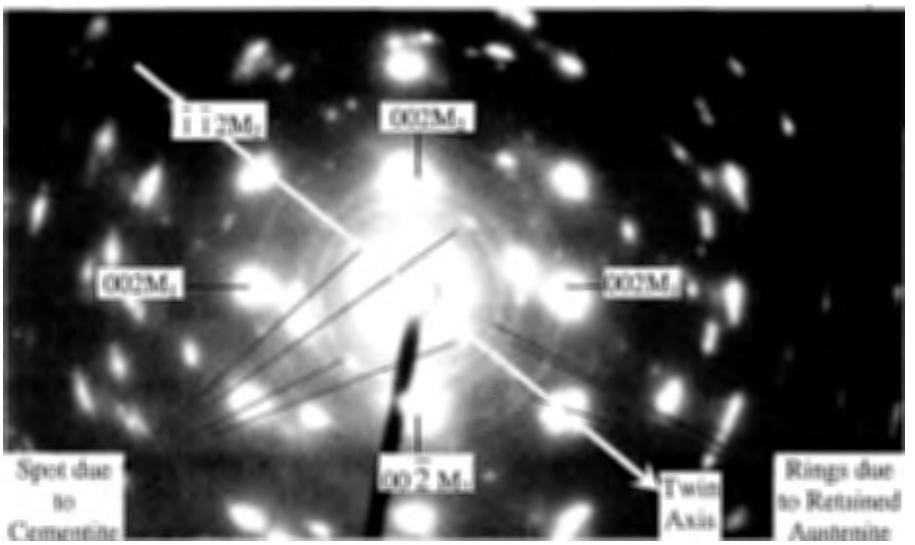

Figure 7.6b Selected area diffraction pattern from twinned section of ground white layer.

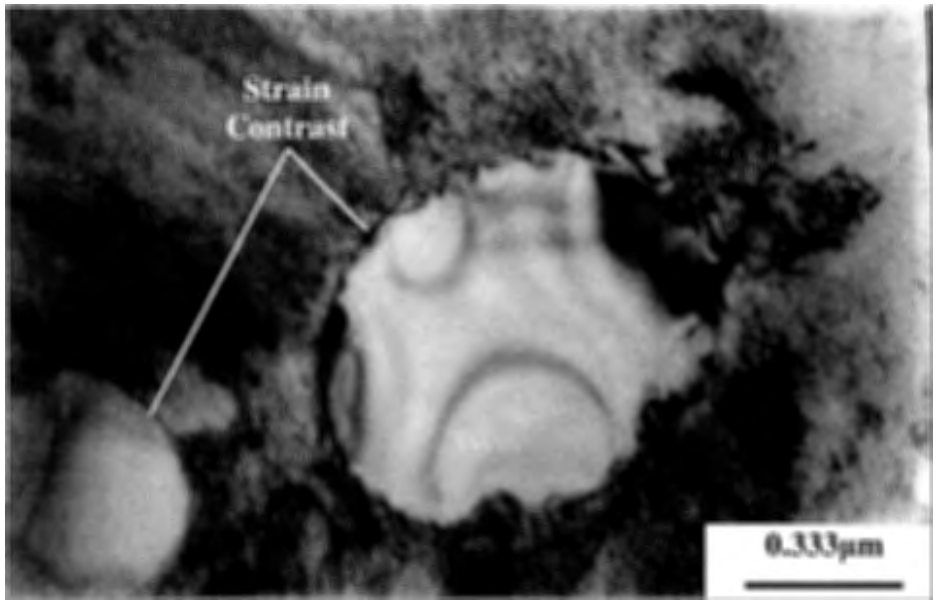

Figure 7.7 TEM Micrograph identifying stain contrast at interface of Fe_3C precipitates and matrix in ground white layer.

7.4.4 Untempered material

The microstructure of the untempered material is basically identical to that observed for the ground white layer as well as of the turned white layer. A typical micrograph Figure 7.8 shows defect bands due to martensite twins and lath like granular morphology of the matrix. A comparative study of the twin density of this sample to those of others indicates that the density in this sample is larger than turned white sample, but smaller than that in ground white layer sample. Cementite precipitates, one of which is shown in Figure 7.9, did not show any orientation relationship with matrix, but also shows exhibited strain associated with martensitic transformation similar to those observed in other samples.

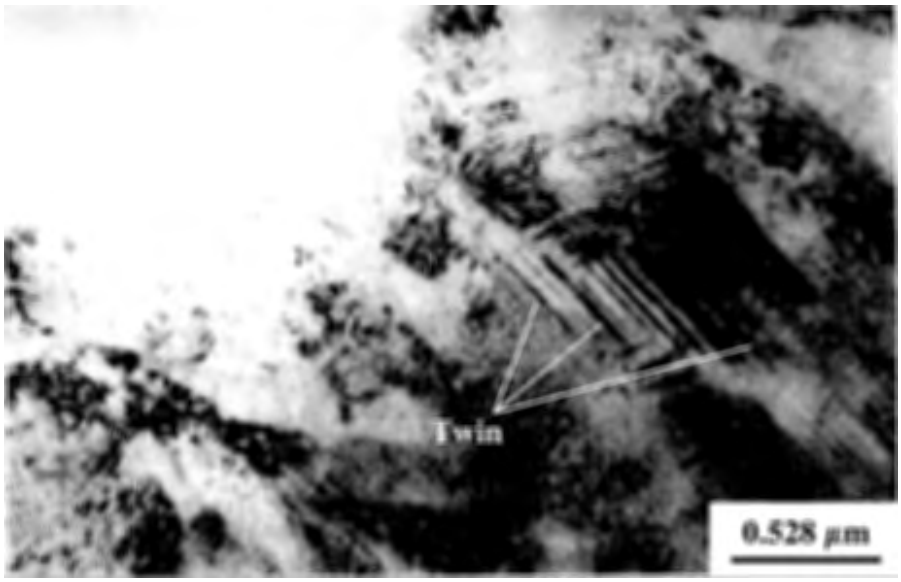

Figure 7.8 Zig-Zag twins of martensite in untempered bulk material

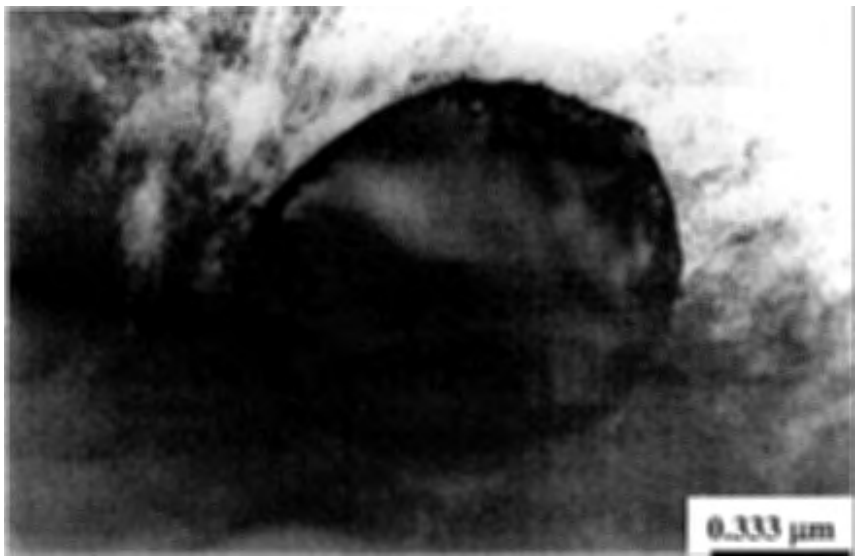

Figure 7.9 Cementite precipitate in untempered bulk material showing no orientation relationship

CHAPTER 8

CONCLUSIONS

Hard turning and grinding experiments have been designed and conducted in this work to generate thick white layers and compare characteristics of the turned white layer versus the ground one. Based on the experimental results, the following conclusions may be drawn:

a) Though both turned and ground surface structures have the white layer, then the dark layer, and followed by the bulk material, the turned white layer appears much more strained in cutting direction than the ground one. The thickness ratio of the dark layer to the white layer for a ground surface is two times more than that of a turned one. In addition, the white/dark layer transition zone is clear for the ground surface but not for the turned one. Further, abusive grinding tends to induce much thicker white layer than hard turning, and the thickest ground white layer only occurs at a certain material removal rate.

b) The characteristics of microhardness profiles for the two types of white layers are similar, in which white layer is much harder than the dark layer, which is slightly softer than the bulk material. The significant difference is that the hardness of ground white layer is about 10 % higher than tuned on, but the ground dark layer is softer

than the turned one. Further etching seems to affect the hardness of bulk material and dark layers.

c) The turned white layer is etch resistant and shows featureless structures in the SEM image, while the ground one is etched and therefore shows clear microstructures. Additionally, the ferrite matrix of the ground dark layer is much more severely etched than the turned one.

d) Both the turned and ground white layers are rich in oxygen or at least oxide-rich. Compared with the bulk material, the significant difference is that the turned white layer has increased carbon and reduced oxygen concentrations, while the ground one behaves just opposite. The variations of other elements are also different for the two types of white layers.

e) XRD studies reveal that samples A, B, C, D, E, and F are martensite in various degrees of tempering. Based on peak widths, the order from most tempered to least tempered is:

   Ground dark layer > Bulk material > Untempered bulk material > Turned white layer > Turned dark layer > Ground white layer

   The results suggest that ground dark layer experienced enough heat during grinding to temper, but not enough heat to form austenite or quench rate to form martensite. The variation in low intensity sharp peaks is not clear yet. The increased width of samples A, B, and C may also be due to plastic deformation.

f) TEM study revealed that a large number of precipitates in turned and ground white layer as compared to bulk material. This suggests that precipitation has occurred due to rapid heating and quenching. No conclusive reason could be suggested for that but

it can be inferred that machining conditions in grinding are more abusive conditions than in hard turning due to which the temperature reached at surface is higher in grinding than in hard turning. The decreasing order or defect structure is:

Ground white layer > Untempered bulk material > Turned white layer > Bulk material

The large number of defect bands in ground white layer as compared to turned white layer suggests that former has fine grain size as compared to later. Precipitates are well crystalline which suggests it was formed after quenching that occurred during machining. Diffused scattering indicates a massive martensitic transformation of the matrix causing atoms to displace from its lattice structure.

REFERENCES

1. Abrão, Alexandre M., Aspinwall, David K., 1996 "The Surface Integrity of Turned and Ground Hardened Bearing Steel," Wear, Vol. 196, pp 279-284.

2. Akcan, N.S., 1998, Microstructure Analysis and Temperature Modeling in Finish Machining of Hard Steels, MS Thesis, Purdue Univesity, West Lafayette, Indiana.

3. Akcan, S., Shah, S., Moylan, S.P., Chhabra, P.N., Chandrasekar, S., Farris, T.N., 1999, "Characteristics of White Layers Formed in Steel by Machining," ASME MED, Vol. 10, 789-795.

4. ASM, 1977, Atlas of Isothermal Transformation & Cooling Transformation Diagrams.

5. Barbacki, A., Kawalec, M., Hormol, A., 2002, "Turning and Grinding as a Source of Microstructural Changes in the Surface Layer of Hardened Steel," Journal of Materials Processing Technology, Vol. 5795, 1-5.

6. Barbacki, A., Kawalec, M., 1997, "Structural Altercations in the Surface White Layer During Hard Machining," Journal of Materials Processing Technology, Vol. 64, pp 33-39.

7. Barry, J., Byrne, G., 2002, "TEM Study on the Surface White Layer in Two Turned Hardened Steels," Journal of Material Science and Engineering, A325, 356-364.

8. Boothroyd, Geofffrey, 1975, Fundamentals of Metal Machining and Machine Tools.

9. Chou, Y., Evans, C.J., 1998, "Process Effects on White Layer Formation in Hard Turning," Transactions of NAMRI/SME, Vol. XXXVI, 117-122.

10. Chou, Y., Evans, C.J., 1999, "White Layer and Thermal Modeling of Hard Turned Surfaces," International Journal of Machine Tools and Manufacturing, Vol. 39, 1863-1881.

11. Chou, Y Kevin, Evans, C.J., Barash, M.M., 2002, "Experimental Investigation on CBN Turning of Hardened AISI 52100 steel," Journal of Materials Processing Technology, Vol. 5834, 1-10.

12. Colwell, L.V., Sinnott, M.J., and Tobin, J.C., 1995, "The Determination of Residual Stresses in Hardened Ground Steel," Journal of the American Society of Mechanical Engineers, Vol. 77, pp 354.

13. Eda, H., Kishi, K., Hashimoto, S., 1981, "The Formation Mechanism of Ground White Layers," Bulletin of JSME, Vol. 24, 743-747.

14. Field, M., Koster, W.P., Kohls, J.B., Snider, R.E., Maranchik, J. Jr., 1970, "Machining of High Strength Steels with Emphasis on Surface Integrity," Metcut Research Associates, Inc., Columbus, Ohio.

15. Field, M., Khales, J.F., 1964, "The Surface Integrity of Machined and Ground High Strength Steels," Defense Metals Information Center Report, Columbus, Ohio, 210, 54-77.

16. Griffiths, B.J., 1985, "White Layer Formations at Machined Surfaces and their Relationship to White Layer Formations at Worn Surfaces," ASME Journal of Tribology, Vol. 107, 165-171.

17. Griffiths, B.J., 1986, "Mechanism of White Layer Generation with Reference to Machining and Deformation Processes," ASME Journal of Tribology, Characteristics of White Layers Formed in Steel by Machining, Vol. 109, 525-530.

18. Griffiths, B.J., Furze, D.C., 1987, "Tribological Advantages of White Layers Produced by Machining," Transactions of ASME, Vol. 109, 338-342.

19. Grozin, B.D. and Iankevich, V.F., Iankevich, 1962, "Friction and Wear in Machinery," Vol. 15, 143.

20. Guo, Y.B. and Sahni, J.S., 2003, "Hard Turning versus Grinding – A Comparative Study of the White Layer Properties," Proc. of NSF Unsolved Problems and Research Needs in Thermal Aspects of Material Removal Processes, Oklahoma State University, Stillwater, Oklahoma, June 10-12.

21. Haidemenopoulos, G.N., Olson, G.B., Cohen, M. Tsuzaki, K., 1989, "Transformation Plasticity of Retained Austenite in Stage-I Tempered Martensite Steels," Scripta Metallurgica, Vol. 23, 207-212.

22. Halverstadt, R.D., 1958, "Analysis of Residual Stress in Ground Surfaces of High Temperature Alloys," American Society of Mechanical Engineers Transactions, Vol. 80, May, 929-940.

23. Harrison, D., 1979, The Corrugation of Railway Rails, Ph.D. Thesis, Cambridge University, England.

24. Helieby-EL, S.O., Rowe, G.W., 1980, "Influence of Surface Roughness and Residual Stress on Fatigue Life of Ground Steel Components," Metals Technology, Vol. 7, 221-225.

25. Henry, Stier, 1988, "The Rewards and Demands of Hard Part Turning," Modern Machine shop, 88-94.

26. Hiroshi EDA,, Kozo KISHI, Santoshi HASHIMOTO, 1981, "The Formation Mechanism of Ground White Layers," Bulletin of the JSME, Vol. 24, No. 190, 743-747.

27. Jatczak, C.F., Larson, J.A., Shin, S.W., 1980, Retained Austenite and its Measurement by X-Ray Diffraction, SAE SP-453, Society of Automobile Engineers, Inc.

28. Juneja, B.L., Sekhon, G.S., 1995, Fundamental of Metal Cutting and Machine Tools.

29. Kalpakjian, S., 1992, Manufacturing Engineering and Technology, 2nd edition.

30. König, W., Berktold, A., Koch, K F., 1993, "Turning versus Grinding: A Comparison of Surface Integrity Aspects and Attainable Accuracies," Annals of CIRP, Vol. 42, 39-43.

31. König, W., Klinger, M., Link, R., 1990, "Machining Hard Materials with Geometrically Defined Cutting Edges – Field of Application and Limitations," Annals of CIRP, Vol. 39, 61-64.

32. Koster, W.P., Filed, M., Fritz, L.J., Gatto, L.R., Kahles, J.F., 1970, "Surface Integrity of Machined Structural Components," Metcut Research Associates, Inc., Columbus, Ohio.

33. Kruth, P., Stevens, L., Froyen, L., Lauwers, B., 1995, "Study of the white layer of a surface machined by die-sinking electro-discharge machining," Annals of CIRP, Vol. 44, 169-172.

34. Kruss, G., 1980, Principles of Heat Treatment of Steel.

35. Kuritsyna, A.D., 1956, "On the Origin of the White Phase on Rubbing Surfaces," Trenie. Iznos., Vol. 11, 182-203.

36. Leskovar, P., 1985, "Investigations of Surface Integrity of Workpieces and Tools," Strojniski Vestnik.

37. Littman, W.E., Wulff, J., 1955, "The Influence of the Grinding Process on the Structure of Hardened Steel," Transactions of ASME, Vol. 47, 692-714.

38. Malkin, S., 1974, "Thermal Aspects of Grinding," Journal of Engineering for Industry, Vol. 96, No. 4, 1177-1183.

39. Matsumoto, Y., Liu, C.R., Barash, M.M., 1984, "Residual Stress in the Machined Surface of Hardened Steel," Proceedings of ASME WAM, High Speed Machining, 193-204.

40. Moulder, J.F., Stickle, W.F., Sobol, P.E., Bomben, K.D., 1995, Handbook of X-Ray Photoelectron Spectroscopy, Physical Electronics, Inc., Eden Prairie, Minnesota.

41. Scott, D., Loy, B., Mills, G.H., 1967, Metallurgical Aspects of Rolling Contact Fatigue, 5th Conference on Lubrication and Wear, London, 181, 94-103.

42. Shaw, M.C., Vyas, A., 1994, "Heat-Affected Zones in Grinding Steel," Annals of CIRP, Vol. 43, 279-282.

43. Stier, H., 1988, "The Rewards and Demands of Hard Part Turning," Modern Machine Shop, 1988, 88-94.

44. Tabor, D., 2000, The Hardness of Metals.

45. Tomlinson, W.J., Blunt, L.A., Spraggett, S., 1991, "The Effect of Workpiece Speed and Grinding Wheel Condition on the Thickness of White Layers Formed on EN 24 Ground Surfaces," Journal of Materials Processing Technology, Vol. 25, 105-110.

46. Tönshoff, H.K., Wobker, H.G., Brandt, D., 1995, "Hard Turning-Influences on the Workpiece Properties," Transactions of NAMRI/SME, Vol. XXIII, 215-220.

47. Trent, E. M., Wright, P.K. 2000, Metal Cutting, Butterworths, London.

48. Turley, D.M., 1975, "The Nature of White-Etching Surface Layers Produced During Reaming Ultra High Strength Steels," Journal of Material Science and Engineering, Vol. 19, 79-86.

49. Vyas, A., Shaw, M.C., 2000 "The Significance of the White Layer in a Hard Turned Steel Chip," Journal of Machining Science and Technology, Vol. 41, 169-175.

50. Wu, D.W., Matsumoto, Y., 1990, "Effect of Harness on Residual Stresses in Orthogonal Machining of AISI 4340 Steel," Journal of Engineering for Industry; Vol. 112, 245-252

51. Xu, L., Kennon, N.F., 1992, "Formation of White Layer During Laboratory Abrasive Wear Testing of Ferrous Alloys," Metals Forum, Vol. 16, 43-49.

52. Yang, Y.Y., Fang, H.S., and Huang, W.G., 1996, "A Study of Wear Resistance of White Layer," Tribology International, Vol. 29, No 5, 425-428.

53. Yokoi, T., Kawasaki, K., Takahashi, M., Koyama, K., Mizui, M., 1996, "Fatigue Properties of High Strength Steels Containing Retained Austenite," Technical Notes, JSAE Review, Vol. 17, 191-212.

54. Yonetani, S., Notoya, H., 1984, "Grinding Residual Stress in Heat Treated High Hardness Steels," Journal of Japan Institute of Metals.

55. Zener, C., Hollman, J.H., 1944, "Effect of Strain Rate upon Plastic Flow of Steel," Journal of Applied Physics, Vol. 15, 23-32.

56. Zhang, B., Shen, W., Liu, Y., Tang, X., Wang, Y., 1997, "Microstructures of Surface White Layer and Internal White Adiabatic Shear Band," Wear, 211, 164-168.

57. Zhu Dong, Wang Fu-Xing, Cai Qi-Gong, Zheng Ming-Xin and Cheng Yin-Quian, 1985, "Effect of retained austenite on rolling element fatigue and its mechanism," Wear, Vol. 105, No.3, 223-234.

APPENDIX 1

A MACHINES, INSTRUMENTS AND THEIR SPECIFICATIONS

CNC Turning Center	**Romi-Hardinge EZ-Path-II**
Controller	Bridgeport "Intelligent DRO" 2-axis control
Distance between center	40 in. (1016 mm)
Spindle nose	A2-6 ASA
Spindle speed range (manual)	4-3,500 rpm
Spindle motor	10hp (continuous) (7.5 kw) AC
Cross slide (X) travel	10.04 in. (255 mm)
Longitudinal (Z) travel	40 in. (1016 mm)
Swing over bed	19.7 in. (500 mm)
Swing over cross slide	9.8 in. (250 mm)
Gardener Surface Grinder	
Optical Microscope	**Olympus BH-2**
Scanning Electron Microscope	**Phillips XL Series XL 30**
Microhardness Tester	**Buehler Micromet 2100 Series**
Model No.	1600-6100
Serial No.	532-MMT1-00281
XPS	**Kratos AXIS 165 Electron Spectrometer**
XRD Diffractometer	**Philips MPD 3040 diffractometer**
Radiation	CrKα
Transmission Electron Microscope	**Hatachi 8000-200 kV**
Ion Miller	Gatan Ion Miller
Model	600
Serial No.	T9051026
Dimpler	**Gatan dimple grinder**
Model	656
Serial No.	T 9051008
Metallographic Polisher	**Buehler Minimet Polisher**
Serial No.	423-MN-5993
Low speed diamond wheel saw	South Bay Technologies

APPENDIX 2

TABLES

B1 Microhardness Measurements for Turned sample (Polished only)

Microhardness Measurements for Turned sample (polished only)								
Apparent distance	True Distance below surface (μm)	Average of vertical and horizontal indentation diagonal (μm)	H1	Average of vertical and horizontal indentation diagonal (μm)	H2	Average of vertical and horizontal indentation diagonal (μm)	H3	Average Hardness
12.70	1.45	7.40	846.42	8.90	585.15	8.00	724.22	718.60
25.40	2.90	7.65	792.00	7.25	881.81	7.65	792.00	821.94
50.80	5.81	7.80	761.83	8.25	680.99	7.78	766.74	736.52
76.20	8.71	8.90	585.15	8.40	656.89	8.30	672.81	638.28
101.60	11.61	12.50	296.64	9.35	530.18	9.15	553.61	460.15
127.00	14.51	9.60	502.93	9.50	513.57	9.75	487.57	501.36
152.40	17.42	9.20	547.61	9.35	530.18	12.25	308.87	462.22
177.80	20.32	9.90	472.91	9.55	508.21	9.25	541.71	507.61
203.20	23.22	9.50	513.57	9.50	513.57	9.20	547.61	524.92
254.00	29.03	9.30	535.90	9.00	572.22	9.00	572.22	560.11
304.80	34.83	9.00	572.22	8.45	649.14	9.40	524.56	581.97
355.60	40.64	8.80	598.53	9.70	492.61	9.15	553.61	548.25
406.40	46.45	9.60	502.93	9.05	565.92	8.95	578.63	549.16
482.60	55.15	11.45	353.54	9.75	487.57	9.55	508.21	449.77
558.80	63.86	9.85	477.72	9.05	565.92	8.90	585.15	542.93
635.00	72.57	9.85	477.72	9.15	553.61	9.15	553.61	528.32

B2 Microhardness Measurements for Turned Sample (Polished and Etched)

Microhardness Measurements for Turned Sample (Polished and Etched)								
Apparent distance	True Distance below surface (μm)	Average (μm)	H1	Average (μm)	H2	Average (μm)	H3	Average Hardness
25.40	3.05	7.50	824.00	6.85	987.80	7.45	835.10	882.30
38.10	4.57	6.80	1002.38	7.10	919.46	6.95	959.58	960.47
50.80	6.10	6.85	987.80	9.60	502.93	7.05	932.55	807.76
63.50	7.62	8.55	634.04	7.40	846.42	8.80	598.53	693.00
76.20	9.14	8.70	612.37	13.85	241.63	8.30	672.81	508.94
88.90	10.67	8.80	598.53	8.60	626.69	10.10	454.37	559.86
101.60	12.19	8.80	598.53	8.80	598.53	9.30	535.90	577.65
114.30	13.72	12.30	306.37	8.70	612.37	8.55	634.04	517.59
127.00	15.24	8.55	634.04	8.40	656.89	8.65	619.47	636.80
139.70	16.76	8.80	598.53	8.85	591.78	8.80	598.53	596.28
152.40	18.29	10.30	436.89	8.85	591.78	8.65	619.47	549.38
165.10	19.81	8.60	626.69	8.70	612.37	11.90	327.31	522.12
177.80	21.34	7.95	733.36	12.15	313.98	8.90	585.15	544.16
190.50	22.86	15.35	196.71	8.10	706.45	8.50	641.52	514.89
203.20	24.38	8.35	664.78	8.35	664.78	10.75	401.08	576.88
215.90	25.91	13.85	241.63	8.50	641.52	11.55	347.44	410.20
228.60	27.43	9.10	559.72	12.50	296.64	8.55	634.04	496.80
241.30	28.96	8.65	619.47	8.20	689.32	8.55	634.04	647.61
254.00	30.48	9.00	572.22	8.70	612.37	8.60	626.69	603.76
279.40	33.53	12.90	278.53	14.95	207.38	13.35	260.07	248.66
304.80	36.58	14.20	229.87	8.70	612.37	12.10	316.58	386.27
355.60	42.67	8.75	605.39	14.55	218.94	15.00	206.00	343.44
406.40	48.77	10.35	432.68	11.55	347.44	11.60	344.46	374.86
482.60	57.91	15.20	200.61	9.35	530.18	9.55	508.21	413.00
558.80	67.06	9.85	477.72	8.80	598.53	12.55	294.28	456.84

B3 Microhardness Measurements for Ground sample (Polished only)

Microhardness Measurements for Ground sample (polished only)							
Depth Below Surface (μm)	Average (μm)	H1	Average (μm)	H2	Average (μm)	H3	Average Hardness
6.35	7.80	761.83	8.10	706.45	8.60	626.69	698.32
12.70	7.25	881.81	7.60	802.46	7.80	761.83	815.37
25.40	7.25	881.81	6.95	959.58	7.05	932.55	924.64
38.10	6.45	1114.12	6.80	1002.38	6.75	1017.28	1044.59
50.80	6.85	987.80	7.05	932.55	6.85	987.80	969.38
63.50	7.10	919.46	7.05	932.55	7.40	846.42	899.48
76.20	7.50	824.00	7.00	945.92	7.00	945.92	905.28
88.90	7.05	932.55	6.35	1149.48	6.65	1048.11	1043.38
101.60	6.35	1149.48	6.35	1149.48	6.50	1097.04	1132.00
127.00	6.65	1048.11	6.45	1114.12	6.45	1114.12	1092.11
152.40	6.70	1032.52	6.50	1097.04	6.45	1114.12	1081.23
177.80	6.40	1131.59	6.65	1048.11	6.70	1032.52	1070.74
203.20	6.50	1097.04	6.50	1097.04	6.45	1114.12	1102.73
228.60	6.65	1048.11	6.60	1064.05	6.45	1114.12	1075.42
254.00	6.50	1097.04	6.25	1186.56	6.45	1114.12	1132.57
304.80	8.30	672.81	7.70	781.75	7.45	835.10	763.22
330.20	8.85	591.78	9.30	535.90	9.60	502.93	543.54
355.60	10.15	449.90	10.10	454.37	10.10	454.37	452.88
406.40	10.15	449.90	9.85	477.72	10.15	449.90	459.18
457.20	10.10	454.37	9.80	482.61	10.10	454.37	463.78
533.40	9.80	482.61	9.75	487.57	10.15	449.90	473.36
609.60	9.90	472.91	9.65	497.73	9.65	497.73	489.46
685.80	9.60	502.93	9.55	508.21	10.10	454.37	488.50
762.00	9.55	508.21	9.35	530.18	9.60	502.93	513.77
838.20	9.60	502.93	9.35	530.18	9.45	519.02	517.38
914.40	9.45	519.02	9.35	530.18	9.35	530.18	526.46
990.60	9.35	530.18	9.00	572.22	9.25	541.71	548.04
1143.00	9.40	524.56	9.20	547.61	8.95	578.63	550.27
1270.00	8.75	605.39	8.55	634.04	8.95	578.63	606.02
1397.00	8.70	612.37	8.30	672.81	8.55	634.04	639.74
1651.00	8.35	664.78	8.55	634.04	8.35	664.78	654.53

B4 Microhardness Measurements for Ground sample (Polished and Etched)

Microhardness Measurements for Ground sample (Polished and Etched)							
Depth Below Surface (μm)	Average (μm)	H1	Average (μm)	H2	Average (μm)	H3	Average Hardness
12.70	6.85	987.80	7.15	906.65	7.05	932.55	942.33
25.40	6.40	1131.59	6.60	1064.05	6.50	1097.04	1097.56
38.10	6.60	1064.05	6.70	1032.52	6.45	1114.12	1070.23
50.80	6.45	1114.12	6.30	1167.80	6.40	1131.59	1137.84
63.50	6.55	1080.36	6.50	1097.04	6.95	959.58	1045.66
76.20	6.40	1131.59	6.85	987.80	6.40	1131.59	1083.66
88.90	6.35	1149.48	6.70	1032.52	6.55	1080.36	1087.45
101.60	7.00	945.92	6.55	1080.36	6.60	1064.05	1030.11
127.00	6.75	1017.28	6.95	959.58	6.30	1167.80	1048.22
152.40	6.55	1080.36	6.80	1002.38	6.70	1032.52	1038.42
177.80	7.45	835.10	6.90	973.53	6.90	973.53	927.39
203.20	7.00	945.92	6.70	1032.52	6.70	1032.52	1003.66
228.60	6.80	1002.38	6.80	1002.38	6.70	1032.52	1012.43
254.00	6.45	1114.12	6.50	1097.04	6.60	1064.05	1091.74
304.80	7.05	932.55	8.65	619.47	6.65	1048.11	866.71
330.20	7.75	771.70	8.80	598.53	7.80	761.83	710.69
355.60	7.90	742.67	8.90	585.15	7.75	771.70	699.84
381.00	12.80	282.90	11.95	324.57	14.75	213.04	273.50
406.40	9.25	541.71	11.45	353.54	10.20	445.50	446.92
431.80	9.50	513.57	11.70	338.59	9.20	547.61	466.59
457.20	13.00	274.26	9.55	508.21	10.65	408.65	397.04
533.40	9.60	502.93	9.45	519.02	9.45	519.02	513.66
609.60	13.25	264.01	10.05	458.90	11.25	366.22	363.04
685.80	13.60	250.59	10.90	390.12	9.85	477.72	372.81
762.00	9.40	524.56	9.15	553.61	9.25	541.71	539.96
838.20	9.25	541.71	9.00	572.22	9.45	519.02	544.32
914.40	8.90	585.15	9.55	508.21	13.40	258.13	450.50
990.60	9.05	565.92	13.30	262.03	9.95	468.17	432.04
1143.00	8.85	591.78	8.85	591.78	8.90	585.15	589.57
1270.00	9.00	572.22	8.55	634.04	7.75	771.70	659.32
1397.00	12.30	306.37	13.35	260.07	12.20	311.41	292.61
1524.00	8.35	664.78	8.40	656.89	8.35	664.78	662.15
1651.00	8.25	680.99	8.40	656.89	10.15	449.90	595.93
1778.00	7.75	771.70	8.25	680.99	8.85	591.78	681.49
1905.00	7.95	733.36	7.85	752.16	12.05	319.21	601.58

B5 Untempered (Polished)

Untempered (polished)			
$H_{diagonal}$	$V_{diagonal}$	Average (μm)	H2
7	7	7	945.91
6.7	6.8	6.75	1017.28
6.6	7	6.8	1002.37
6.9	7	6.95	959.57
6.9	6.9	6.9	973.53
6.7	6.5	6.6	1064.04
6.8	7	6.9	973.53

B6 Untempered (Polished and Etched)

Untempered (Polished and Etched)			
$H_{diagonal}$	$V_{diagonal}$	Average (μm)	H2
6.4	5.7	6.05	1266.30
6.5	6.4	6.45	1114.11
6.2	5.8	6	1287.5
6.5	6	6.25	1186.56
6.6	6.4	6.5	1097.04
6.3	6.4	6.35	1149.48
6	5.5	5.75	1401.89
6.3	5.8	6.05	1266.30
6	6.1	6.05	1266.30
6.2	5.5	5.85	1354.37